Available online at www.sciencedirect.com

ScienceDirect

Journal of Ocean Engineering and Science 4 (2019) 352–372

www.elsevier.com/locate/joes

Original Article

Static behavior of offshore two-planar tubular KT-joints under axial loading at fire-induced elevated temperatures

Neda Azari-Dodaran, Hamid Ahmadi*

Faculty of Civil Engineering, University of Tabriz, Tabriz 5166616471, Iran

Received 18 March 2019; received in revised form 26 May 2019; accepted 28 May 2019
Available online 12 June 2019

Abstract

A total of 540 nonlinear steady-state finite element analyses were performed to study the influence of temperature and dimensionless geometrical parameters (β, γ, θ, and τ) on the ultimate strength, failure modes, and initial stiffness of two-planar tubular KT-joints. The joints were analyzed under two types of axial loading and five different temperatures (20 °C, 200 °C, 400 °C, 550 °C, and 700 °C). So far, there has not been any equation available for calculating the ultimate strength of two-planar tubular KT-joints at elevated temperatures. Hence, after parametric study, a set of design formulas were developed through nonlinear regression analyses, to calculate the ultimate strength of two-planar tubular KT-joints subjected to axial loading at elevated temperatures.

Keywords: Ultimate strength; Two-planar tubular KT-joint; Axial loading; Elevated temperatures; Parametric equation.

1. Introduction

The presence of multi-planar connections, e.g. two planar tubular KT-joints studied in the present paper, is an intrinsic feature of offshore tubular structures such as jacket-type platforms and jack-up rigs. These structures are mainly fabricated from circular hollow section (CHS) members due to their plenty of advantages such as high strength-to-weight ratio, attractive appearance, rapid erection, low drag coefficient, and easy fabrication [1–3]. In such structures, the CHS members, also called tubular elements, are connected together by welding the prepared ends of the braces onto the undisturbed surface of the chord forming a tubular joint. As a result of geometric discontinuity and complexity in stress distribution at the connections, tubular joints require greater attention than other components to ensure structural integrity [4].

To study the behavior of tubular joints and to relate this behavior easily to the geometrical properties of the connection, a set of dimensionless geometrical parameters has been defined: β (brace-to-chord diameter ratio), γ (chord wall slenderness ratio), θ (brace inclination angle), τ (brace-to-chord wall thickness ratio), and ζ (relative gap). Fig. 1 shows a two-planar tubular KT-joint with the geometric parameters for chord and brace diameters D and d, and the corresponding wall thicknesses T and t.

Although multi-planar joints cover the majority of practical applications, studies on their ultimate strength even at ambient temperature are rather limited due to the complexity and high cost involved. Makino et al. [5] tested 20 KK connections and identified two failure modes occurring when the connection is symmetrically loaded. Paul et al. [6] conducted a parametric study to investigate the static strength of two planar KK joints under axial loading; and proposed two equations (one for each failure mode) for calculating the ultimate capacity of two-planar KK joint at ambient temperature. Lee and Wilmshurst [7,8] conducted a numerical study on the static strength of KK-joints and established a finite element model. Recently, Forti et al. [9] conducted a parametric study on symmetrically loaded multi-planar KK-joints and proposed analytical expressions to predict the strength of the joint at ambient temperature.

* Corresponding author.
E-mail addresses: azari_neda@yahoo.com (N. Azari-Dodaran), h-ahmadi@tabrizu.ac.ir (H. Ahmadi).

https://doi.org/10.1016/j.joes.2019.05.009

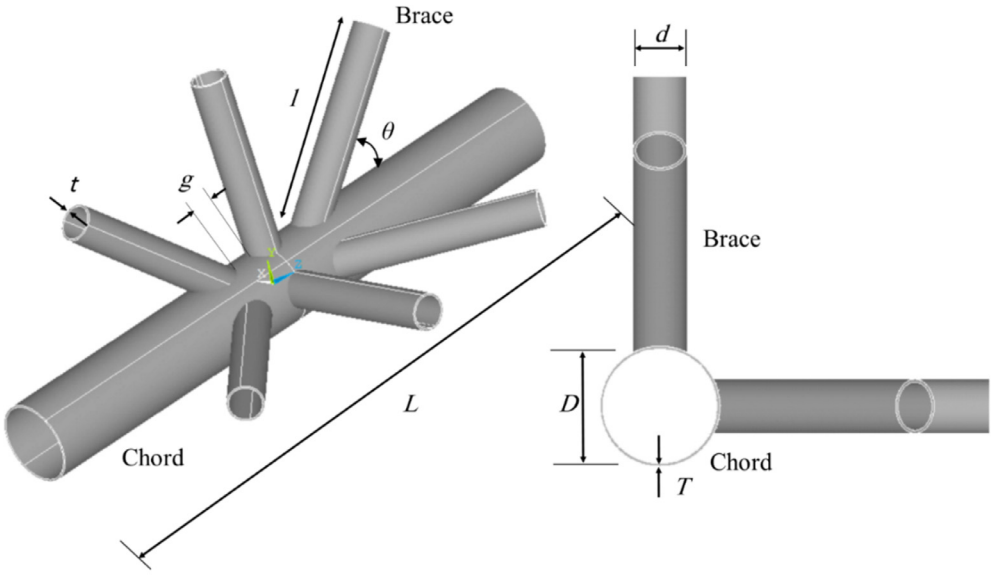

Fig. 1. Geometrical notation for a two-planar tubular KT-joint.

Mechanical characteristics of the steel material deteriorate greatly at high temperature. Hence, at elevated temperatures, a tubular joint may fail subjected to a load far below its static strength at ambient temperature. Consequently, the entire structure might collapse after the failure of one or several tubular joints in fire. Therefore, the study of tubular joint's performance at elevated temperatures is a topic of interest. Following paragraphs review the recent studies on the ultimate strength of tubular joints at elevated temperatures.

Ozyurt et al. [10] conducted an extensive parametric study on static behavior of T-, Y-, X-, N- and non-overlapped K-joints under axial loading at high temperature. They compared the results of numerical FE analysis with corresponding values obtained from design formulas proposed by CIDECT design guide [11] and EN 1993-1-8 [12] through replacing the yield strength or the elastic modulus of steel material at ambient temperature with the corresponding values at high temperatures. Liu et al. [13] investigated the mechanical behavior ring-stiffened T-joints at high temperature. Yu et al. [14] investigated the influence of the impact load on the mechanical behavior of tubular T-joints through experimental investigation. Xu et al. [15] developed an artificial neural network to calculate the ultimate strength of tubular T-joints at elevated temperatures. Chen et al. [16] conducted both experimental and numerical investigations to study the fire resistance of CHS T-joints stiffened with internal rings subjected to axial compression at high temperature. Gao et al. [17] conducted an experimental and numerical study to investigate the strength of tubular T-joints reinforced with collar plates under fire condition. Fung et al. [18] studied the performance of circular hollow section T-joints under in-plane loading at elevated temperatures. Shao et al. [19,20] discussed two techniques for predicting the static strength of tubular T-joints and studied the static strength for CHS tubular K-joints under fire condition. Ozyurt and Wang [21] presented a numerical investigation on the resistance of axially loaded T- and X-joints composed of elliptical hollow section (EHS) members at elevated temperatures.

Some of the more recent works on static behavior of tubular joints at elevated temperatures include: Azari Dodaran et al. [22,23] on K- and KT-joints, Lan et al. [24] on stainless steel gap and overlapped K- and N-joints, He et al. [25–27] on K-joints, Lan et al. [28] on internally crown- and saddle-stiffened DT-, T-, and Y-joints, Lan and Huang [29] on X- and T-joints, Tan et al. [4], Shao et al. [30], Jin et al. [31,32] and Chen et al. [33] on T-joints, and Liu et al. [34] on steel planar tubular trusses, among others.

Preceding discussion indicates that the majority of research works on the behavior of tubular structures at elevated temperatures have focused on uniplanar joints. However, as mentioned before, the presence of multi-planar joints is an intrinsic feature of offshore tubular structures and the multi-planarity might have an important effect on the strength of the joint. Thus for multi-planar connections, the parametric formula of simple uniplanar tubular joints may not be applicable for the strength prediction at elevated temperatures, since such formula may lead to highly over- or under-predicting results. Nevertheless, as far as the authors are aware, for multi-planar joints which cover the majority of practical applications, no comprehensive study on the strength under fire condition has been reported due to the complexity and high cost involved.

Although two-planar tubular KT-joint is a quite common joint type found in steel offshore structures, the strength of two-planar tubular KT-joint at elevated temperatures has not been investigated so far and no design equation is available to determine the ultimate strength for this type of joints under the fire condition.

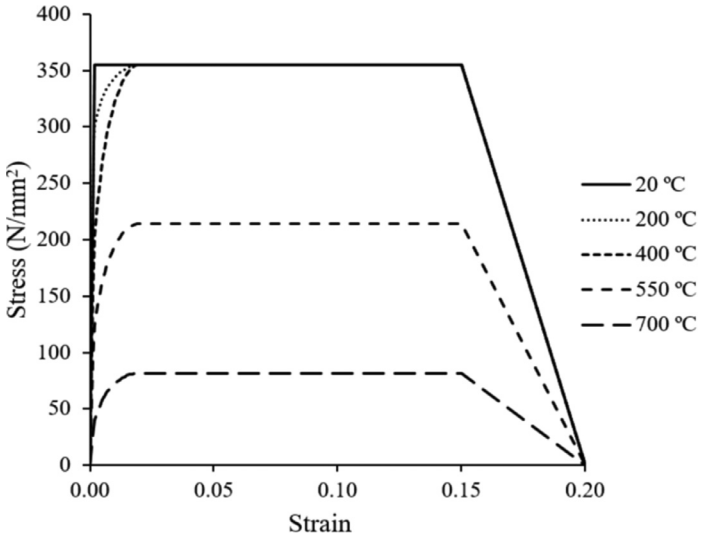

Fig. 2. Material model of steel at high temperatures.

In the present paper, results of a numerical parametric investigation on the structural behavior of two-planar tubular KT-joints under the axial loading at elevated temperatures are presented and discussed. A total of 540 nonlinear steady-state finite element (FE) analyses were performed on 54 FE models to investigate the influence of temperature and dimensionless geometrical parameters of the two-planar tubular KT-joint on its ultimate strength, initial stiffness and failure modes. Dimensionless geometrical parameters (β, γ, τ, α, θ and α_B), used to relate the behavior of a tubular joint to its geometrical properties, are defined in Fig. 1. Developed FE model was verified against available experimental data reported by Tan et al. [4]. After the parametric study, a set of design equations was developed, through nonlinear regression analyses, for calculating the ultimate strength of two-planar tubular KT-joints subjected to both types of axial loading.

2. FE strategy

The FE method as an efficient numerical procedure for solving problems of engineering and mathematical physics was adopted in the present research to study the structural behavior of tubular joints. This section present the details of modeling the material properties, simulation of the weld profile, definition of boundary conditions, mesh generation procedure, analysis method, and validation of the FE results.

2.1. Material behavior

In the present investigation, the von Mises yield criterion and isotropic strain hardening plasticity model were applied. The yield stress of steel material (f_y) at ambient temperature was taken 355 N/mm^2. The material properties belong to the steel grade S355 (EN10210 S355J2H). The Young's modulus of 206 GPa and Poisson's ratio of 0.3 were used for modeling the material of the chord and braces. The high temperature stress-strain relationship was specified according to EN 1993-1-2 [35] as shown in Fig. 2. For accurate definition of plastic behavior of material by considering the actual (instantaneous) dimensions, true stress and strain should be used. Hence, the stress-strain relationships were converted to true stress-strain relationships according to the following formulas:

$$\varepsilon_T = \ln(1+\varepsilon) \tag{1}$$

$$\sigma_T = \sigma(1+\varepsilon) \tag{2}$$

where ε_T and ε are true and engineering strains, respectively; and σ_T and σ are true and engineering stresses, respectively.

It should be noted that the value of elongation for all types of steel varies with the temperature. For more information on the mechanical response of the steel at elevated temperatures and extreme cooling conditions, the reader is referred for example to Mirmomeni et al. [36] and Azhari et al. [37,38], among others.

2.2. Weld profile

The influence of weld modeling on the joint strength mostly depends on the difference between the actual real projected gap between the brace toes and the apparent gap between the weld toes [39]. Therefore, it is important to include weld modeling for the joints with a small gap size and a large weld size, as the large weld could notably decrease the small gap size [24]. In addition, Fung et al. [40] studied the influence of weld modeling on ultimate strength and suggested the FE simulation without the weld modeling because it gave a lower ultimate strength than the experimental data. In their investigation, the difference in the ultimate strength between the joints with and without the weld was nearly 10%. Furthermore, the difference in the load-displacement curve was found to be less than 10%. Because the influence of weld modeling on the joint strength is insignificant, the weld modeling was not included in the present research. For more information

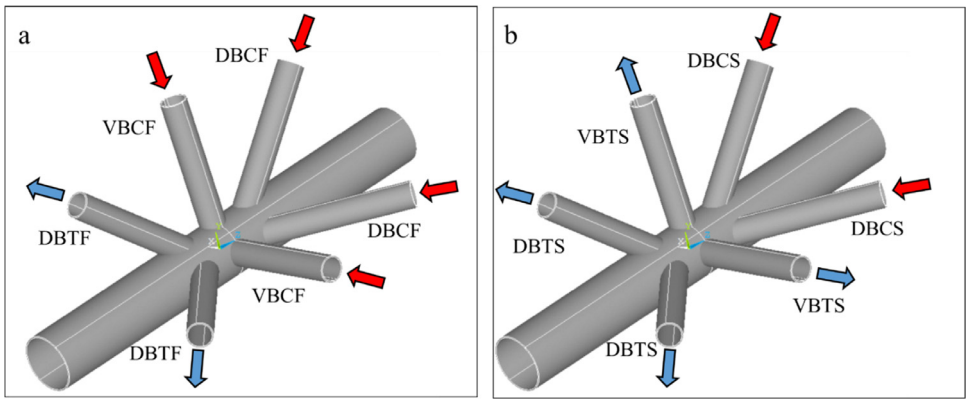

Fig. 3. (a) The first type of loading, and (b) The second type of loading.

about the effects of the weld on the mechanical properties of high strength and ultra-high strength steel tubes in fabricated hybrid sections, the reader is referred to Javidan et al. [41]. A complementary discussion on the effect of the weld profile has been provided in Section 2.6.

2.3. Applied loads and mechanical boundary condition

The chord ends fixity condition in tubular joints of offshore structures ranges from almost fixed to almost pinned with generally being closer to almost fixed [42]. In the view of the fact the influence of the chord end restraints on the stress distribution at the brace-to-chord intersection is only notable for joints with $\alpha < 8$ and high β and γ values [43,44], which do not generally observed practically. Both ends of the chord were completely restrained. For more information about boundary condition at ambient temperature, the reader is referred to Choo et al. [45]. Tan et al. [4] investigated the influence of boundary condition on the ultimate load of tubular T-joints at high temperatures. In spite of the fact that they found as the temperature becomes greater, the difference between pinned-end and fixed-end conditions increases, they eventually suggested the fixed-end condition to display the real behavior of the joint. In the numerical model, for defining chord ends fixity condition, the nodes at both chord ends were selected, then all degrees of freedom of the selected nodes were constrained.

Two different types of axial loading were applied to the models. The difference between them was the type of axial loading applied on the vertical braces. The vertical braces are subjected to axial compressive and tensile load in the first and second types of loading, respectively (Fig. 3). The names assigned to the braces are shown in Fig. 3. The name of each brace indicates a combination of loading type, brace geometry, and applied load. For example, VBCF means vertical brace (VB) subjected to brace axial compression (C) under the first type of loading (F) and DBTS means diagonal brace (DB) subjected to brace axial tension (T) under the second type of loading (S).

To ensure that the stress at the brace-to-chord intersection is not influenced by the chord end situation, a long-enough chord that is greater than six times the chord diameter ($\alpha \geq 12$) is utilized. In consequence, a value of $\alpha = 16$ was taken for all joint in the parametric investigation. The stress distribution around the brace-to-chord intersection is not affected by the length of the chord [25]. In the present work, α_B was assumed to be 10. The ends of braces were assumed to be free. Because of the symmetry in the geometry of the

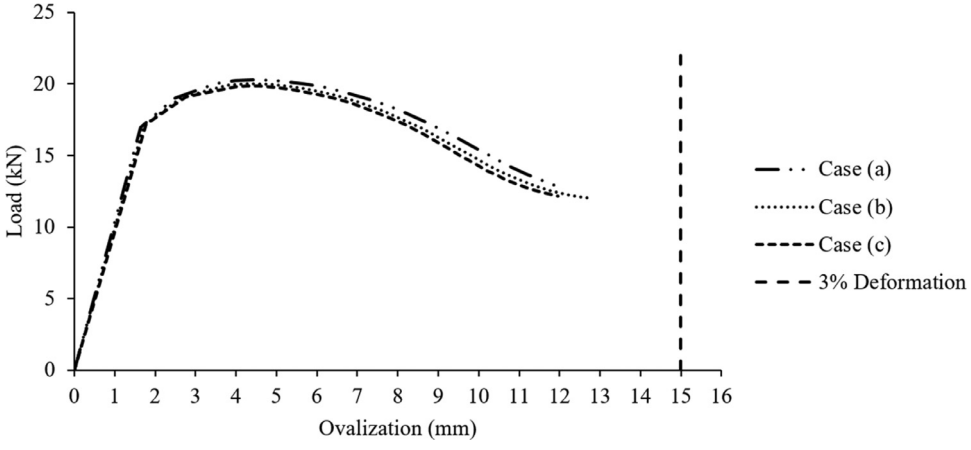

Fig. 4. Results of the mesh convergence study.

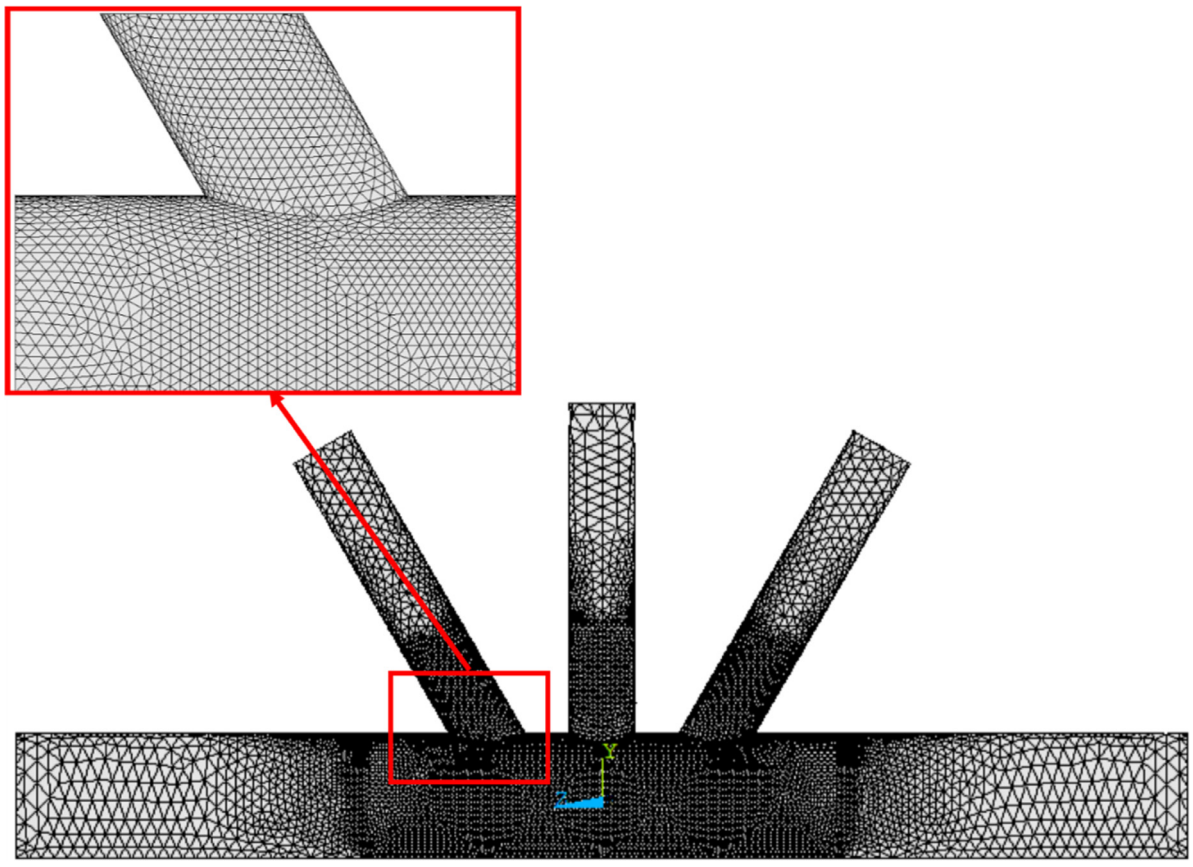

Fig. 5. FE mesh layout for half of an entire two-planar CHS KT-joint.

Table 1
Mesh convergence examination results.

Case	Mesh size (mm)		Ultimate Strength (kN)	Ultimate strength / Ultimate strength of case *c*
	Joint zone	Outside the joint zone		
a	20	50	20.31	1.02
b	15	45	20.02	1.01
c	12	40	19.86	1.00

connection and anti-symmetry in loading condition, only one fourth of the entire joint was modeled and appropriate symmetric/antisymmetric boundary conditions were defined on respective symmetry/antisymmetry planes.

2.4. Mesh convergence

The FE ANSYS Ver. 17 [46] element type SOLID186 was utilized to simulate the tubular joints at elevated temperatures. SOLID186 element is described by 20 nodes having three degrees of freedom for each node. To determine the most appropriate mesh size for the analysis, a mesh convergence investigation was performed. The same mesh size was then applied to all models. The two-planar tubular KT-joint was divided to two regions including joint zone and outside the joint zone. Fig. 4 and Table 1 present the results of mesh sensitivity investigation. It was concluded that the suitable mesh sizes were 15 and 45 mm for the joint zone and outside the joint zone, respectively (Case *b* in Table 1). Fig. 5 demonstrates the FE mesh layout for a sample two-planar KT-joint.

2.5. Analysis

The steady-state analysis was utilized in which the load was applied to the joint at particular steady high temperature up to the time that the failure happened. In this study, both material and geometric nonlinearities were considered in FE analysis. FE model of the present study is not able to consider the effect of fracture failure. For more information, the reader is referred to Cofer and Will [47], Dexter and Lee [48], Qian et al. [49], Ma et al. [50], and Gu et al. [51], among others. In tubular joints under axial loading, the load-displacement curve usually grows to a maximum point and then decreases. In these cases, the typical procedures fail to

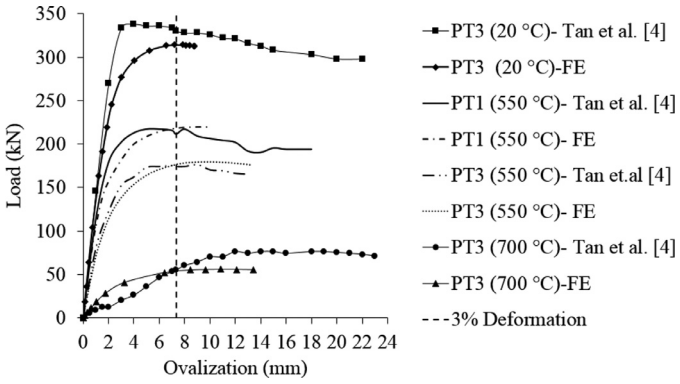

Fig. 6. Comparing the load-ovalization curves of test specimens and FE models (PT3).

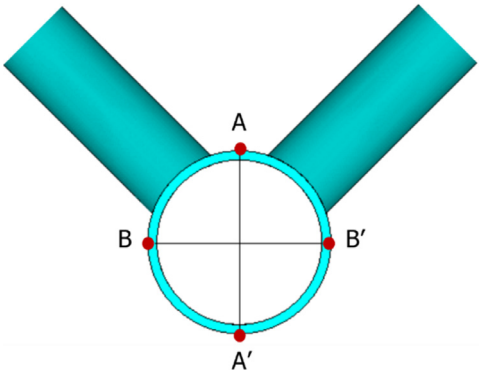

Fig. 7. Extension of Lu et al. [49] criterion to multi-planar joints by Forti et al. [9].

converge. Furthermore, to overcome the numerical stability, the arc-length method was utilized in the present work. For more information about the arc-length method, the reader is referred to Kohnke [52].

2.6. Verification

The precision of FE results for estimating the ultimate strength of two-planar tubular KT-joints at elevated temperatures should be validated against experimental test data. It should be noted that no database of ultimate strength for two-planar tubular KT-joints under axial load at elevated temperatures is available in the literature. Hence, the available experimental test results of Tan et al. [4] at ambient and elevated temperatures were used to validate the numerical modeling of two-planar tubular KT-joints under axial load at high temperature. Geometrical parameters of the joints tested Tan et al. [4] have been given in Table 2.

Fig. 6 compares the load-displacement curves exerted from the present FE analysis and the test data provided by Tan et al. [4] at ambient and elevated temperatures. As shown in Fig. 6, there is a good agreement between the vertical displacement, stiffness and ultimate strength extracted from experimental results of Tan et al. [4] and the predictions of the validating FE model. The values of the ultimate capacity achieved from numerical and experimental models are compared in Table 3. Numerical results have a good agreement with the experimental data, with an average FE/test result ratio of 0.97 and a standard deviation of 2.72%. From the results shown in Fig. 6 and Table 3, it can be concluded that the developed FE model is capable of producing valid results with acceptable accuracy.

As mentioned in Section 2.2, the weld modeling was not included in the FE models of present research due to its insignificant influence on the ultimate load. Table 4 compares the values of ultimate load for the joints with and without the weld modeling. It can been seen that the difference between the strength values is less than 5% and hence the inclusion of the weld profile is not necessary.

Table 2
Geometrical dimensions of the joints tested by Tan et al. [4] used for FE model verification.

Joint name	T (°C)	D (mm)	T (mm)	L (mm)	d (mm)	T (mm)	l (mm)	β (d/D)
PT1	550	244.5	6.3	2200	195.6	6.3	1100	0.80
	20							
PT3	550	244.5	6.3	2200	168.7	6.3	1100	0.69
	700							

Table 3
Results of the verification study.

Joint name	Temperature (°C)	Joint strength (kN)		
		Present FE model	Test [4]	FE/Test
PT1	550	217.94	217	1.004
	20	318.06	338	0.941
PT3	550	174.31	175	0.996
	700	52.38	55	0.952

Table 4
Comparing the ultimate load of the joints with and without the weld modeling.

Joint name	Temperature (°C)	Joint strength (kN)		
		With weld modeling	Without weld modeling	Difference (%)
PT1	550	228.01	217.94	4.62
PT3	20	333.90	318.06	4.98
	550	178.23	174.31	2.25
	700	54.92	52.38	4.85

3. Effects of geometry and temperature on the static behavior

3.1. Details of parametric investigation

An extensive numerical investigation on two-planar tubular KT-joints was conducted to study the influence of geometrical parameters and temperature on static behavior of two-planar KT-joints under axial loading at high temperatures. Different values assigned to geometrical parameters (Table 5) cover the practical range of usage for these parameters typically found in tubular joints of offshore structures. Parametric study included 540 FE analyses carried out on 54 two-planar

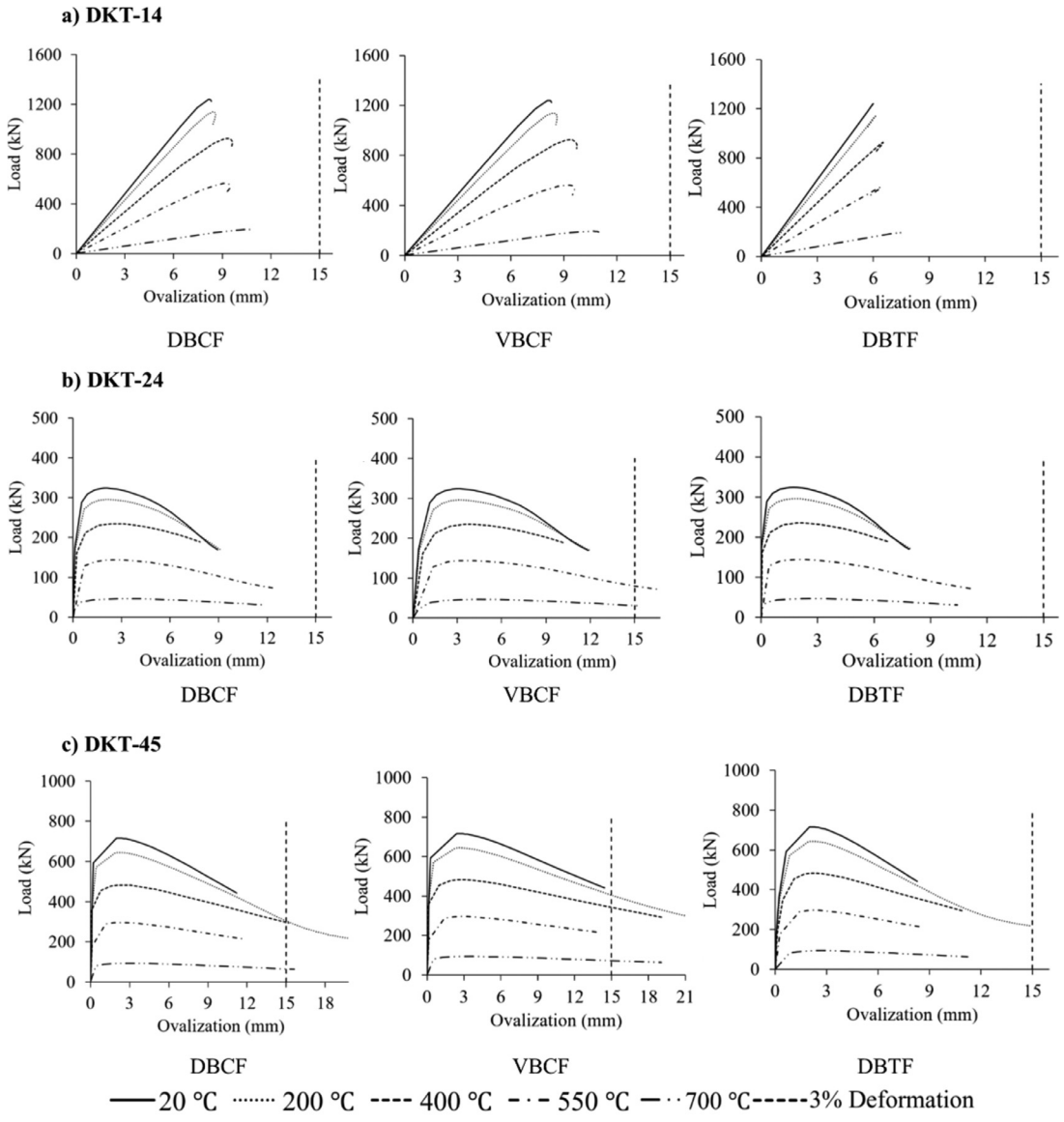

Fig. 8. The influence of temperature on the static strength and initial stiffness of two-planar tubular KT-joints under the first type of loading.

Table 5
Values of dimensional and non-dimensional parameters for the parametric investigation.

Parameter	Expression	Value(s)
L	Chord length	4 m
D	Chord diameter	0.5 m
α	$2L/D$	16
α_B	$2l/d$	10
β	d/D	0.3, 0.45, 0.6
γ	$D/2T$	10, 20, 30
θ	Brace-to-chord intersection angle	30°, 45°, 60°
τ	t/T	0.4, 1.0
g	Gap size	0.15 m

KT-joint configurations (Table 6) at five different temperatures (20, 200, 400, 550, and 700 °C). The 20 °C is ambient temperature and the reasons for selecting the other values for the temperature are as follows: At 200 °C, steel starts to lose its initial stiffness; at 400 °C, its yield strength starts to decrease, and there is no hardening on its plasticity; at 550 °C, there are significant reductions in both yield strength and stiffness; and at 700 °C, steel almost entirely loses its strength [4].

3.2. Failure criteria

In order to determine the ultimate load, Lu et al. [53] proposed a deformation limit of $0.03D$ indentation of the chord wall (relative to the chord centerline). Forti et al. [9] extended this deformation limit to multi-planar joints. The criterion was given by the relative displacement of diametrically opposed nodes divided by the chord diameter:

$$\varepsilon_{\text{diametral}} = \frac{\mu_2 - \mu_1}{D} \tag{3}$$

where μ_1 and μ_2 are the horizontal displacement of nodes B and B' or the vertical displacement of nodes A and A' shown

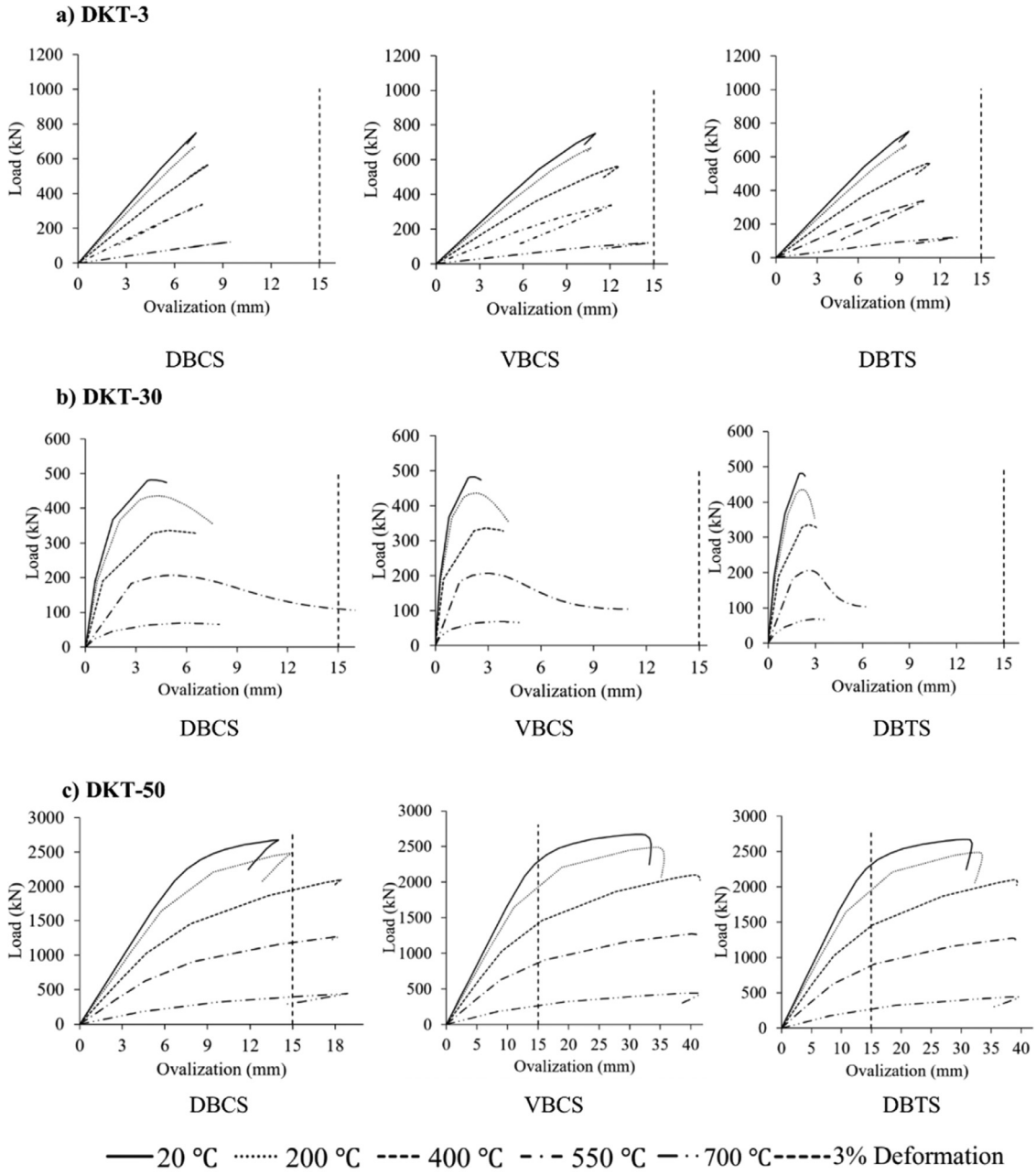

Fig. 9. The influence of temperature on the static strength and initial stiffness of two-planar tubular KT-joints under the second type of loading.

in Fig. 7. The diametric deformation is limited to 0.03D. Ultimate load is defined by the peak load or the load at the deformation of 0.03D in load-deformation curves whichever is smaller.

3.3. The effect of the temperature on the ultimate strength and initial stiffness

Figs. 8 and 9, as an example, show the load-deformation curves for all of three braces in six two-planar KT-joints under the first and the second types of loading, respectively. Loading types and brace names have been described in Fig. 3. It can be seen that by increasing the temperature, both the initial stiffness and ultimate load decrease for a two-planar KT-joint. The average amounts of strength reduction under the first and second types of loading are tabulated in Table 7. It can be concluded that the joint strength reduction under the first type of loading is smaller than the corresponding value under the second type of loading.

3.4. The effect of the β on the ultimate strength and initial stiffness

Results of investigating the effect of the β on the static strength are presented in this section. The parameter β is the ratio of the brace diameter (d) to the chord diameter (D). To

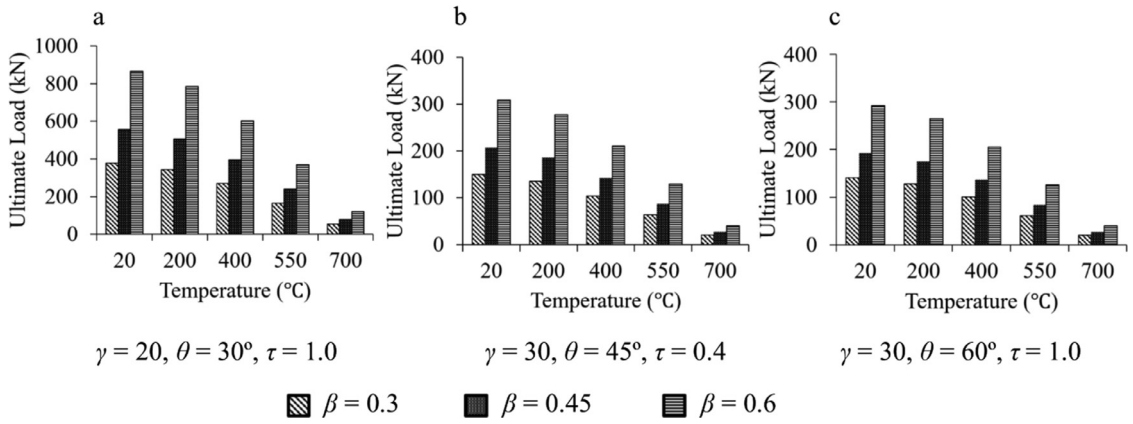

Fig. 10. The influence of the β on the ultimate load of two-planar tubular KT-joints at ambient and high temperatures under the first type of loading.

Table 6
Geometrical properties of two-planar KT-joint models considered for numerical parametric investigation.

Joint name	D (m)	α	β	γ	τ	θ	Joint name	D (m)	α	β	γ	τ	θ
DKT-1	0.5	16	0.3	10	0.4	30°	DKT-28	0.5	16	0.45	20	1.0	45°
DKT-2	0.5	16	0.3	10	1.0	30°	DKT-29	0.5	16	0.45	30	0.4	45°
DKT-3	0.5	16	0.3	20	0.4	30°	DKT-30	0.5	16	0.45	30	1.0	45°
DKT-4	0.5	16	0.3	20	1.0	30°	DKT-31	0.5	16	0.45	10	0.4	60°
DKT-5	0.5	16	0.3	30	0.4	30°	DKT-32	0.5	16	0.45	10	1.0	60°
DKT-6	0.5	16	0.3	30	1.0	30°	DKT-33	0.5	16	0.45	20	0.4	60°
DKT-7	0.5	16	0.3	10	0.4	45°	DKT-34	0.5	16	0.45	20	1.0	60°
DKT-8	0.5	16	0.3	10	1.0	45°	DKT-35	0.5	16	0.45	30	0.4	60°
DKT-9	0.5	16	0.3	20	0.4	45°	DKT-36	0.5	16	0.45	30	1.0	60°
DKT-10	0.5	16	0.3	20	1.0	45°	DKT-37	0.5	16	0.6	10	0.4	30°
DKT-11	0.5	16	0.3	30	0.4	45°	DKT-38	0.5	16	0.6	10	1.0	30°
DKT-12	0.5	16	0.3	30	1.0	45°	DKT-39	0.5	16	0.6	20	0.4	30°
DKT-13	0.5	16	0.3	10	0.4	60°	DKT-40	0.5	16	0.6	20	1.0	30°
DKT-14	0.5	16	0.3	10	1.0	60°	DKT-41	0.5	16	0.6	30	0.4	30°
DKT-15	0.5	16	0.3	20	0.4	60°	DKT-42	0.5	16	0.6	30	1.0	30°
DKT-16	0.5	16	0.3	20	1.0	60°	DKT-43	0.5	16	0.6	10	0.4	45°
DKT-17	0.5	16	0.3	30	0.4	60°	DKT-44	0.5	16	0.6	10	1.0	45°
DKT-18	0.5	16	0.3	30	1.0	60°	DKT-45	0.5	16	0.6	20	0.4	45°
DKT-19	0.5	16	0.45	10	0.4	30°	DKT-46	0.5	16	0.6	20	1.0	45°
DKT-20	0.5	16	0.45	10	1.0	30°	DKT-47	0.5	16	0.6	30	0.4	45°
DKT-21	0.5	16	0.45	20	0.4	30°	DKT-48	0.5	16	0.6	30	1.0	45°
DKT-22	0.5	16	0.45	20	1.0	30°	DKT-49	0.5	16	0.6	10	0.4	60°
DKT-23	0.5	16	0.45	30	0.4	30°	DKT-50	0.5	16	0.6	10	1.0	60°
DKT-24	0.5	16	0.45	30	1.0	30°	DKT-51	0.5	16	0.6	20	0.4	60°
DKT-25	0.5	16	0.45	10	0.4	45°	DKT-52	0.5	16	0.6	20	1.0	60°
DKT-26	0.5	16	0.45	10	1.0	45°	DKT-53	0.5	16	0.6	30	0.4	60°
DKT-27	0.5	16	0.45	20	0.4	45°	DKT-54	0.5	16	0.6	30	1.0	60°

Table 7
The average joint bearing capacity reduction at different high temperatures.

Temperature (°C)	R_{UT}	
	First type of loading	Second type of loading
20	1.00	1.00
200	0.90	0.89
400	0.70	0.67
550	0.42	0.42
700	0.14	0.13

Note: R_{UT} = the ratio of ultimate strength at elevated temperature to ultimate strength at ambient temperature.

study the influence of the β on the structural behavior, three different values (0.3, 0.45, and 0.6) were designated to the β. The increase of the β leads to the increase of the ultimate load at all temperatures (Figs. 10 and 11). The reason is that by increasing the β in a model having fixed value of the chord diameter, the diameter of the brace member is increased; and subsequently the value of the ultimate load increases. It was also found that the increase of the β leads to the increase of the joint's initial stiffness at all temperatures under the second type of loading (Fig. 12). The same trend was observed for the joints under the first type of loading.

3.5. The effect of the γ on the ultimate strength and initial stiffness

Six charts are presented in Figs. 13 and 14 showing the change of the ultimate strength due to the change of the γ

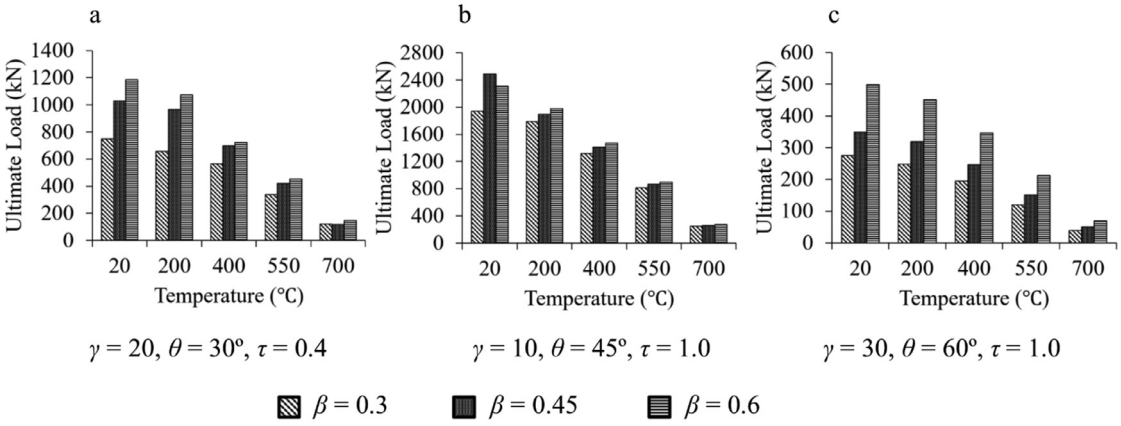

Fig. 11. The influence of the β on the ultimate load of two-planar tubular KT-joints at ambient and high temperatures under the second type of loading.

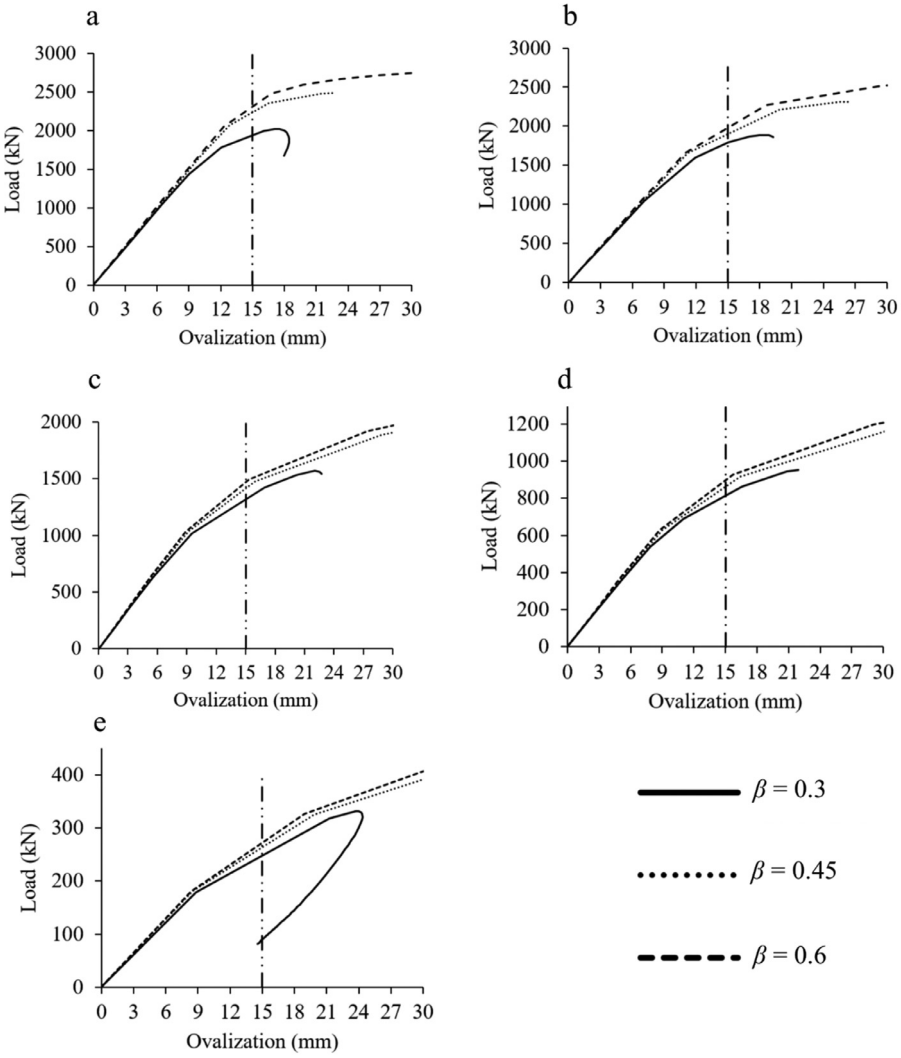

Fig. 12. The influence of the β on the initial stiffness of two-planar tubular KT-joints under the second type of loading ($\gamma = 10$, $\tau = 1.0$, $\theta = 45°$): (a) 20 °C, (b) 200 °C, (c) 400 °C, (d) 550 °C, (e) 700 °C.

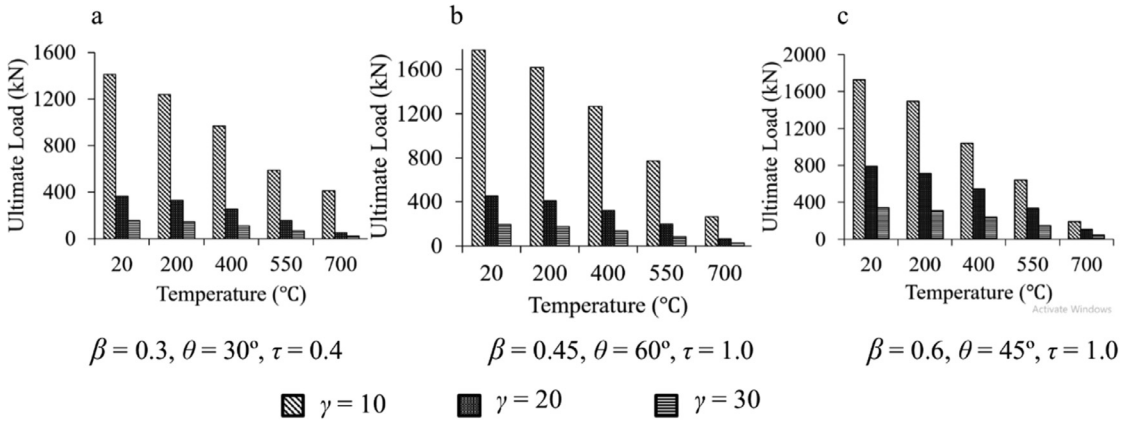

Fig. 13. The influence of the γ on the ultimate load of two-planar tubular KT-joints at ambient and high temperatures under the first type of loading.

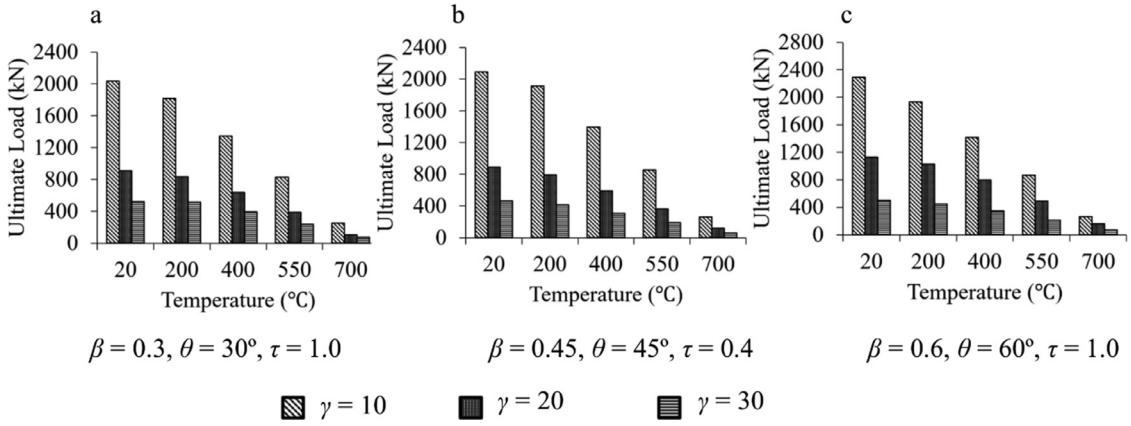

Fig. 14. The influence of the γ on the ultimate load of two-planar tubular KT-joints at ambient and high temperatures under the second type of loading.

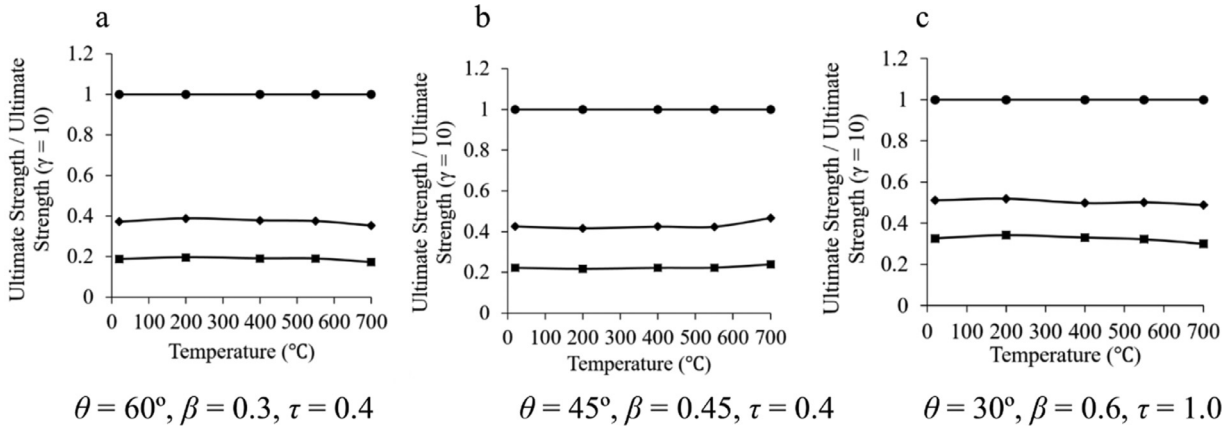

Fig. 15. Relative ultimate load of two-planar tubular KT-joints with different values of the γ under the second type of loading at ambient and high temperatures.

under the first and second type of loading, respectively. It can be observed that at all temperatures, the value of the ultimate strength decreases by increasing the γ; and the amount of the strength reduction from the joints with $\gamma = 10$ to the joints with $\gamma = 20$ is bigger than the strength reduction from $\gamma = 20$ to $\gamma = 30$.

In Fig. 15, the ultimate strength is non-dimensionalized with respect to the ultimate strength of the case with $\gamma = 10$ at different temperatures under the second type of loading. It can be seen that the influence of the γ on the ultimate strength is independent from the temperature. The same trend was observed for the joints under the second type of loading.

Five charts are presented in Fig. 16 indicating the effect of the γ on the initial stiffness under the first type of loading. It can be seen that by increasing the γ, the initial stiffness

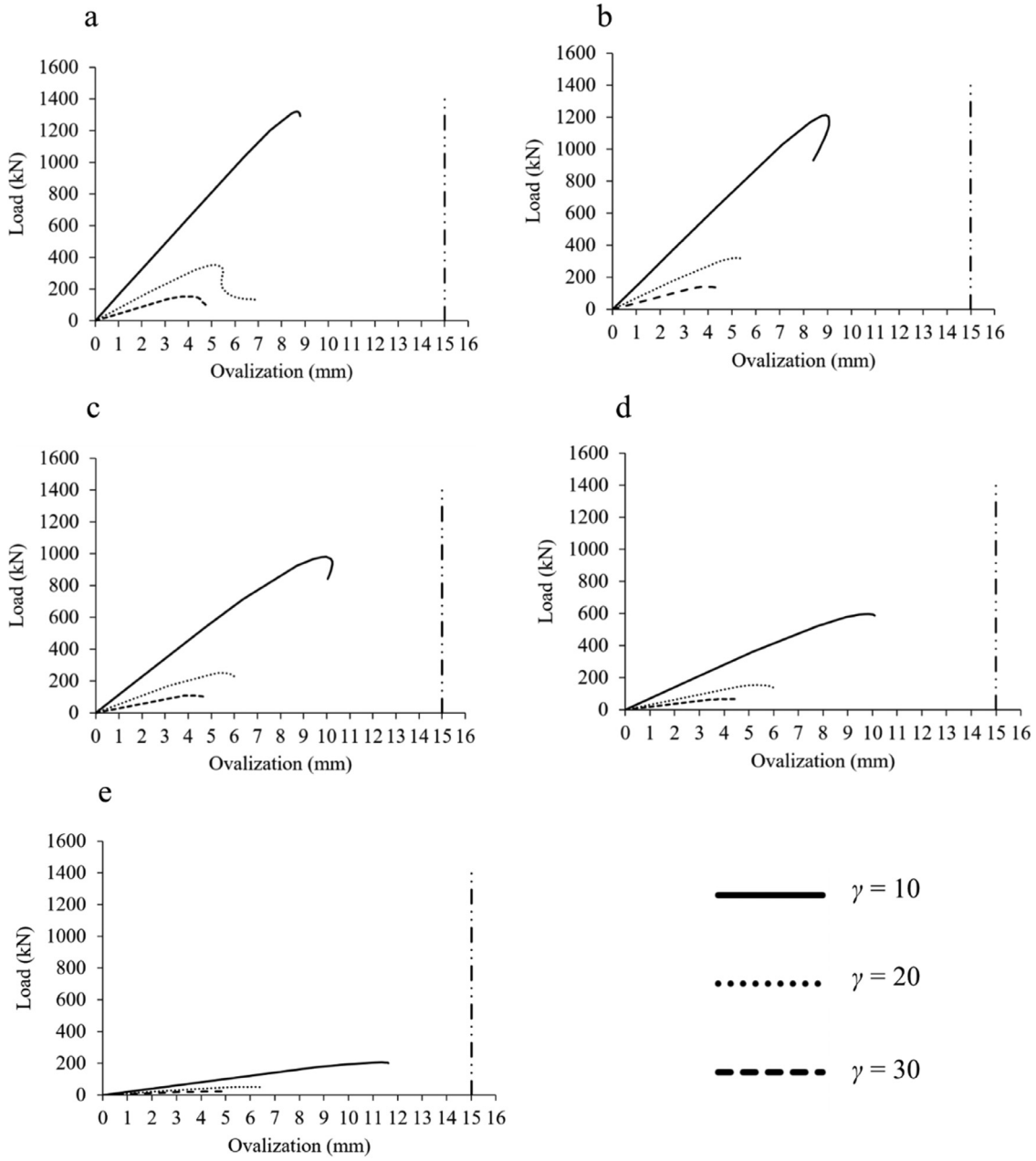

Fig. 16. The influence of γ on the initial stiffness of two-planar tubular KT-joints under the first type of loading ($\beta = 0.3$, $\tau = 1.0$, $\theta = 45°$): (a) 20 °C, (b) 200 °C, (c) 400 °C, (d) 550 °C, (e) 700 °C.

decreases at all temperatures. The same trend was observed for the joints under the second type of loading.

3.6. The influence of the θ on the ultimate load and initial stiffness

For investigating the influence of the brace inclination angle (θ), three different values (30°, 45° and 60°) were picked for the θ. The θ has no considerable influence on the static load (Figs. 17 and 18). It can also be said that temperature has no effect over the influence of the θ on the ultimate load (Fig. 19). There is no significant difference among the values of the initial stiffness in models having different values of the θ under the first type of loading (Fig. 20). The same trend was observed for the joints under the second type of loading.

3.7. The influence of the τ on the ultimate load and initial stiffness

If the γ remains constant, the increase of the τ ($= t/T$) in a model with fixed chord thickness leads to the increase of the brace thickness which consequently results in bigger values of the ultimate load. As it was expected, the ultimate load increases with the increase of the τ (Figs. 21 and 22). Fig. 23 depicts the influence of the τ on the initial stiffness at 20 °C, 200 °C, 400 °C, 550 °C, and 700 °C under the second

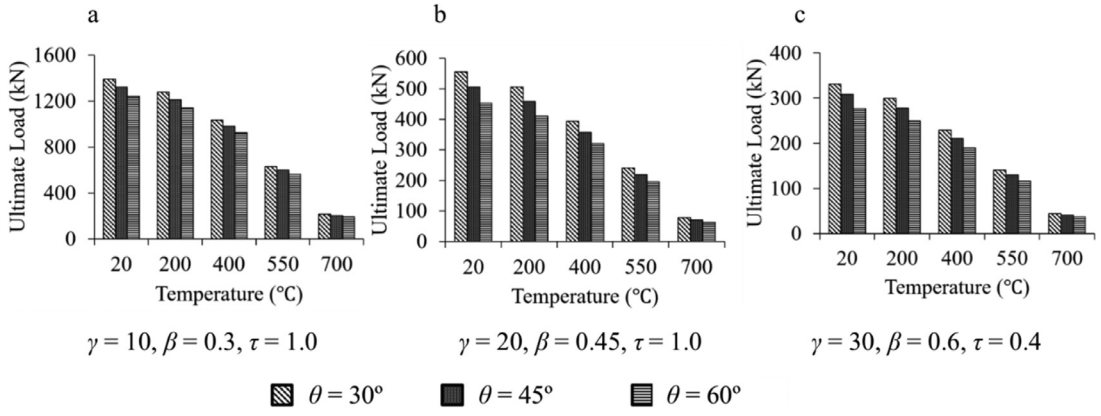

Fig. 17. The influence of θ on the ultimate load of two-planar tubular KT-joints at ambient and high temperatures under the first type of loading.

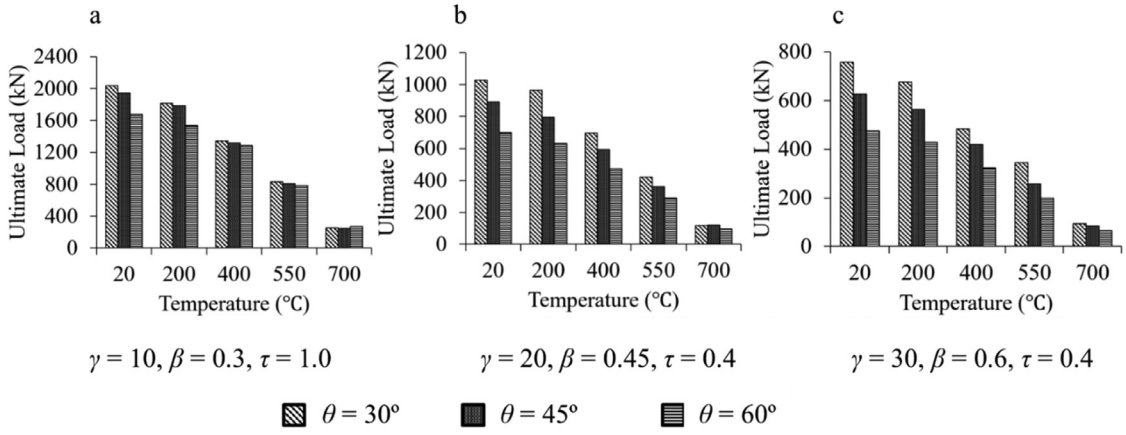

Fig. 18. The influence of θ on the ultimate load of two-planar tubular KT-joints at ambient and high temperatures under the second type of loading.

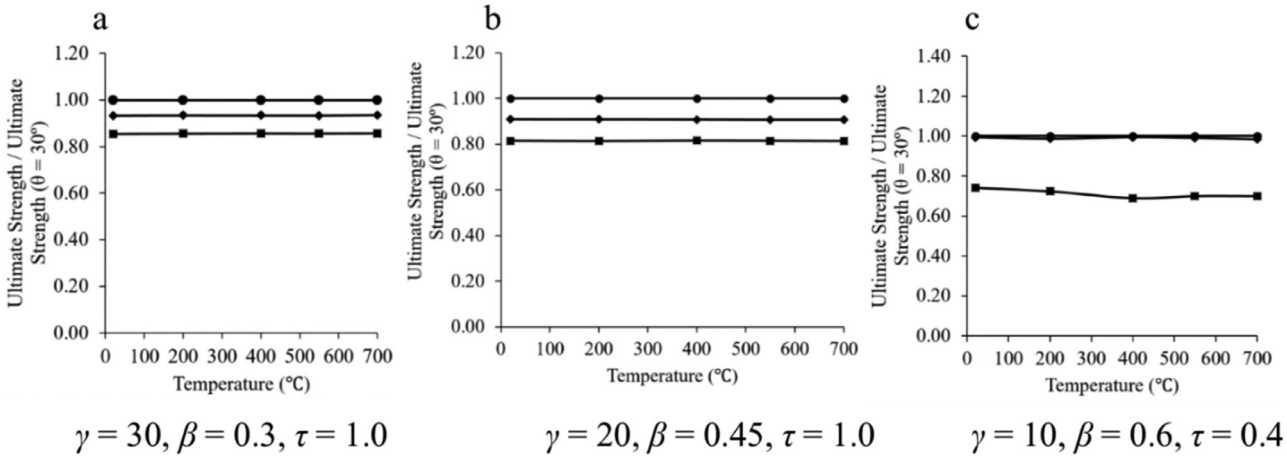

Fig. 19. Relative ultimate load of two-planar tubular KT-joints with different values of the θ at high temperatures under the first type of loading.

type of loading. As can be seen, increasing the τ has no significant effect on initial stiffness. The same results were observed for the joints under the first type of loading.

3.8. The influence of the geometrical parameters on failure modes of two-planar KT-joints

The geometrical parameters affect the failure mode of two-planar tubular KT-joints. In the present investigation, three types of failure mode were observed including chord wall plastification, brace local buckling, and combined chord wall plastification and brace local buckling. The most common type of failure mode as shown in Fig. 24 is wall plastification around the brace-to-chord intersection. The second type of failure mode is the brace local buckling that seen more in the joints with relatively small β and τ (Fig. 25). Another failure mode that was only observed in nearly 25% of the joints under the second type of loading is the

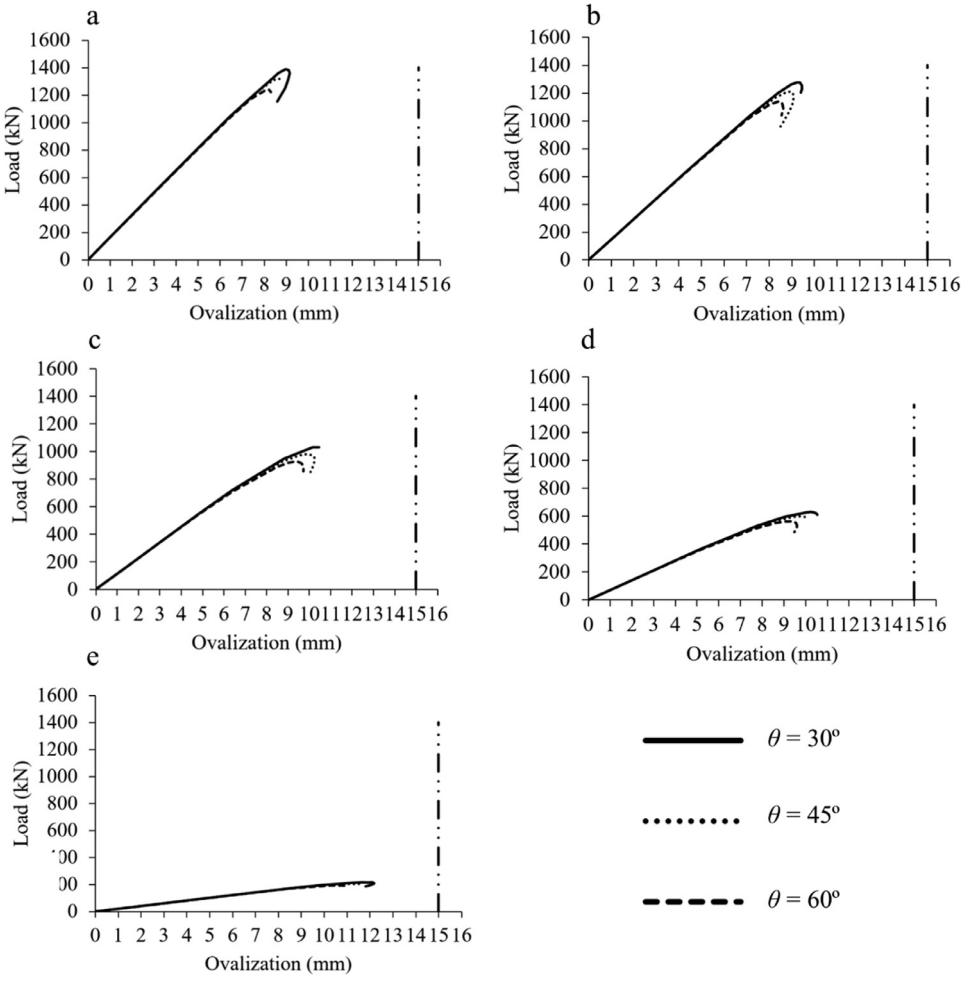

Fig. 20. The effect of θ on the initial stiffness of two-planar tubular KT-joints under the first type of loading ($\beta = 0.3$, $\tau = 1.0$, $\gamma = 10$): (a) 20 °C, (b) 200 °C, (c) 400 °C, (d) 550 °C, (e) 700 °C.

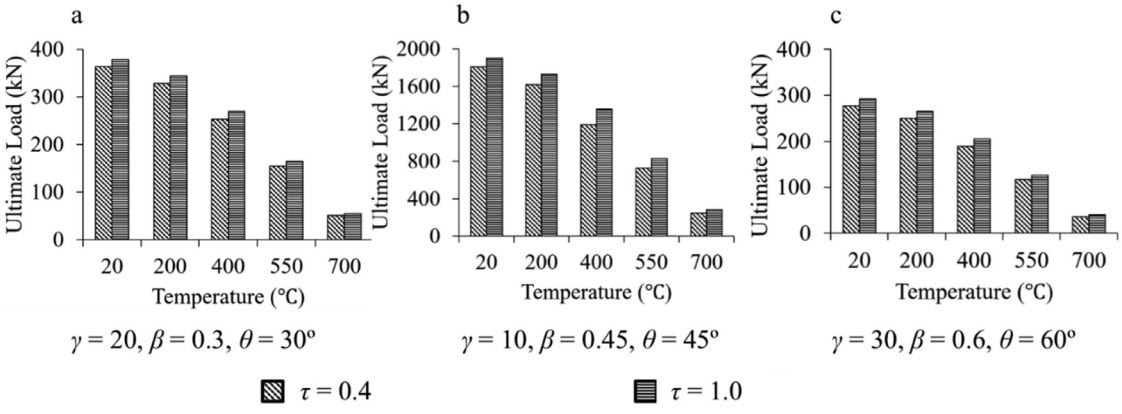

Fig. 21. The influence of the τ on the ultimate load of two-planar tubular KK-joints at ambient and high temperatures under the first type of loading.

combination of wall plastification and brace local buckling. Tables 8 and 9 summarize the results of the effect of the geometrical parameters on the type of failure modes for two-planar KT-joints under the first and second types of loading, respectively.

3.9. The influence of the multi-planarity on the ultimate load

Table 10, as an example, compares the ultimate load values of three uniplanar and two-planar KT-joints with the same geometrical parameters under both studied load cases. As it can

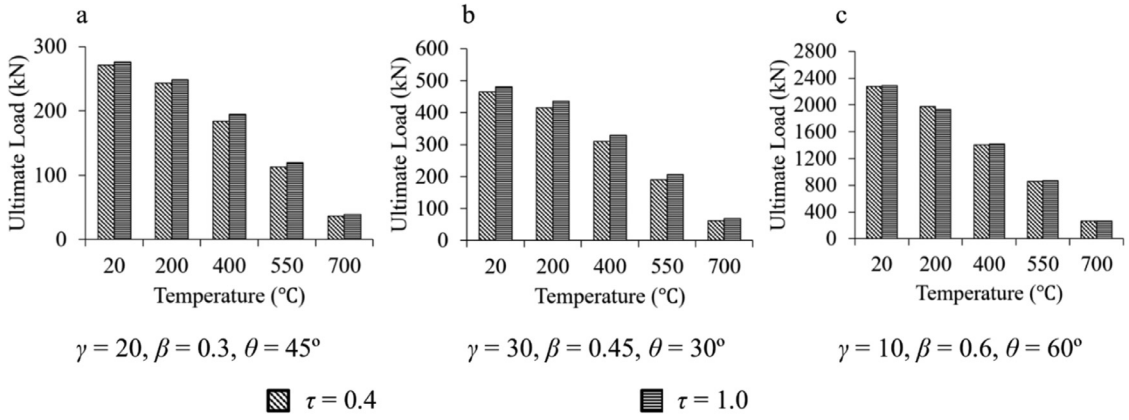

Fig. 22. The influence of the τ on the ultimate load of two-planar tubular KK-joints at ambient and high temperatures under the second type of loading.

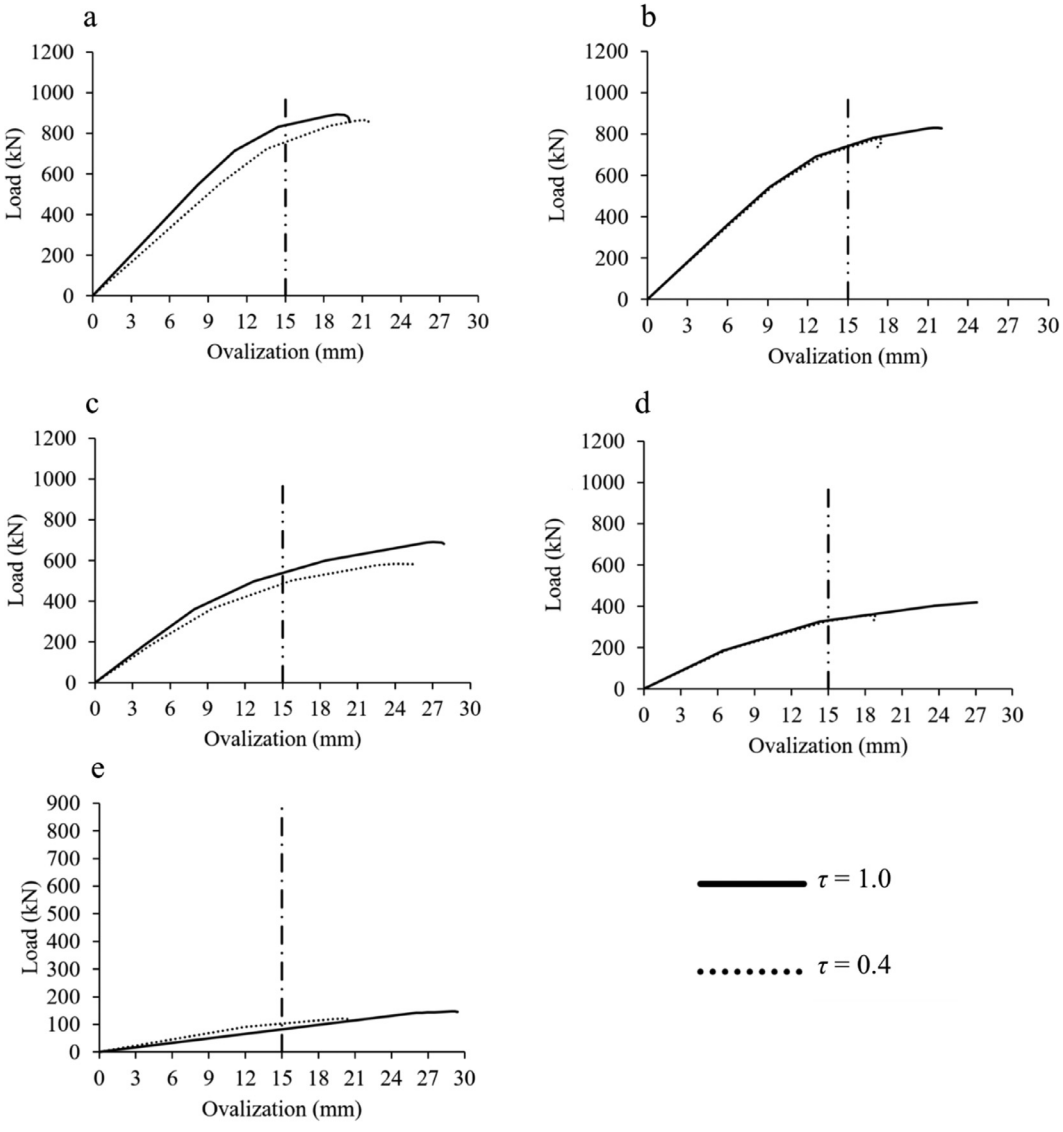

Fig. 23. The influence of the τ on the initial stiffness of two-planar tubular KT-joints under the second type of loading ($\beta = 0.6$, $\theta = 30°$, $\gamma = 30$): (a) 20 °C, (b) 200 °C, (c) 400 °C, (d) 550 °C, (e) 700 °C.

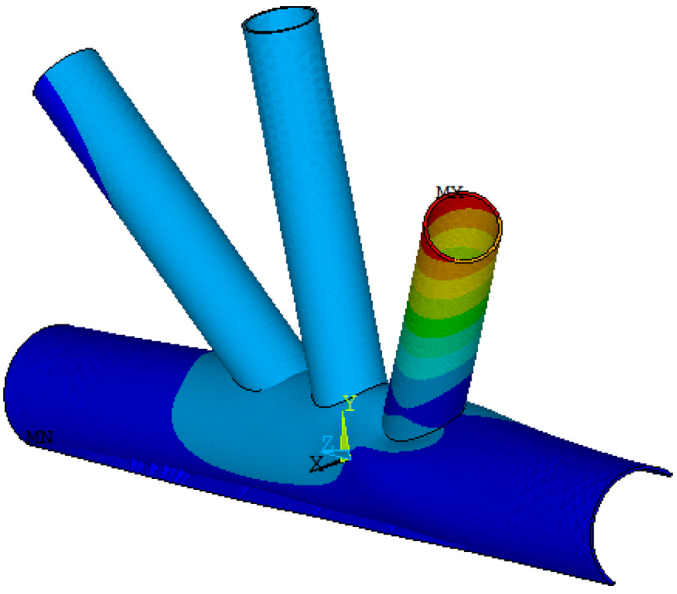

Fig. 24. Failure mode *A*: Chord wall plastification (Scale factor: 5).

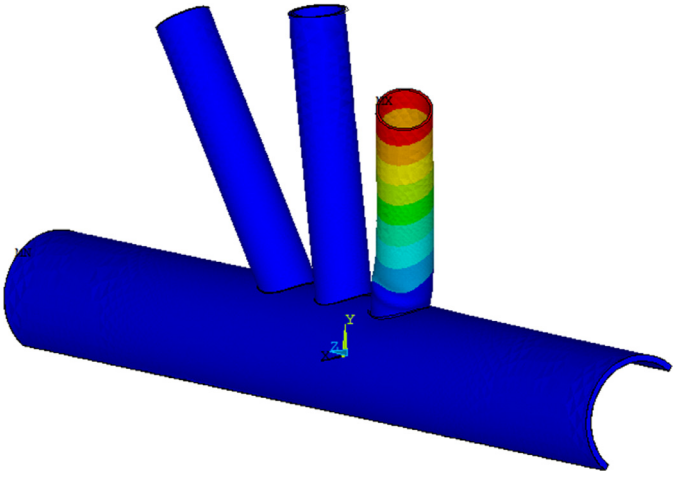

Fig. 25. Failure mode *B*: Brace local buckling (Scale factor: 5).

be seen, there are significant differences between the ultimate load values in uniplanar KT-joints and the corresponding values in two-planar connections. Hence, it can be said that the multi-planarity has remarkable effect on the ultimate strength of the KT-joint.

Table 8
The effect of the geometrical parameters on failure modes of two-planar KT-joints under the first type of loading.

β	θ	γ	$\tau=0.4$	$\tau=1.0$
0.3	30°	10 & 20	Mode B	Mode A
		30	Mode A	Mode A
	45°	10	Mode B	Mode A
		20 & 30	Mode A	Mode A
	60°	10	Mode B	Mode A
		20 & 30	Mode A	Mode A
0.45 & 0.6	30°	10	Mode B	Mode A
		20 & 30	Mode A	Mode A
	45° & 60°	all	Mode A	Mode A

Table 9
The effect of the geometrical parameters on failure modes of two-planar KT-joints under the second type of loading.

β	θ	γ	$\tau=0.4$	$\tau=1.0$
0.3	30°	all	Mode B	Mode A
	45° & 60°	10 & 20	Mode B	Mode A
		30	Mode B	Mode B
0.45	30°	10 & 20	Mode B	Mode A
		30	Mode AB	Mode A
	45°	10	Mode B	Mode A
		20	Mode AB	Mode A
		30	Mode AB	Mode AB
	60°	10 & 20	Mode AB	Mode A
		30	Mode AB	Mode AB
0.6	30°	all	Mode A	Mode A
	45° & 60°	10	Mode A	Mode A
		20	Mode AB	Mode A
		30	Mode AB	Mode AB

4. Derivation of parametric equations for the prediction of the ultimate strength

Using FE analysis for estimating the ultimate strength of two-planar tubular KT-joints is a time consuming process. In contrast, parametric equations presenting the ultimate strength as a function of dimensionless geometrical parameters can be quite useful for design purposes. Until now, no design equation has been proposed for calculating the ultimate strength of two-planar tubular KT-joints under axial loading at elevated temperatures.

For each failure mode, the FE database was divided into two sets: a training dataset and a testing dataset. Nearly 90% of the whole FE data was implemented for the training, i.e.

Table 10
Comparison of the ultimate load between uniplanar and two-planar KT-joints.

Joint name	T (°C)	Type of loading	Ultimate load (kN)		Ultimate Strength (two-planar) /Ultimate Strength (uniplanar)
			Uniplanar	Two-planar	
DKT-16	550	First	188.83	142.09	0.75
DKT-16	550	Second	269.15	239.16	0.89
DKT-22	700	First	91.99	123.50	1.34
DKT-22	700	Second	67.13	78.76	1.17
DKT-48	400	First	330.76	474.54	1.43
DKT-48	400	Second	396.04	458.08	1.16

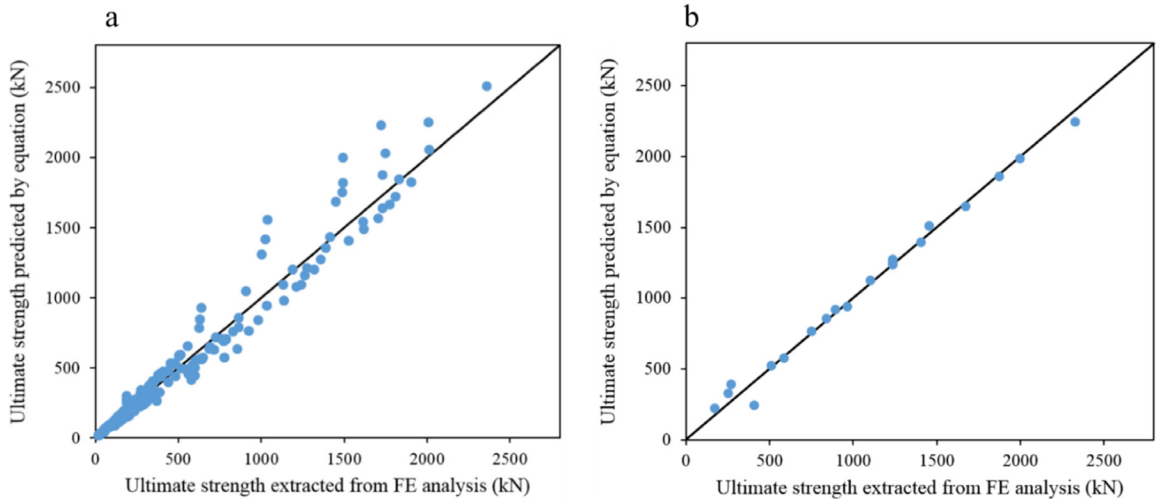

Fig. 26. Comparison of the ultimate strength predicted by the proposed equations with the corresponding training data extracted from FE analyses (the first type of loading): (a) Eq. (4), (b) Eq. (5).

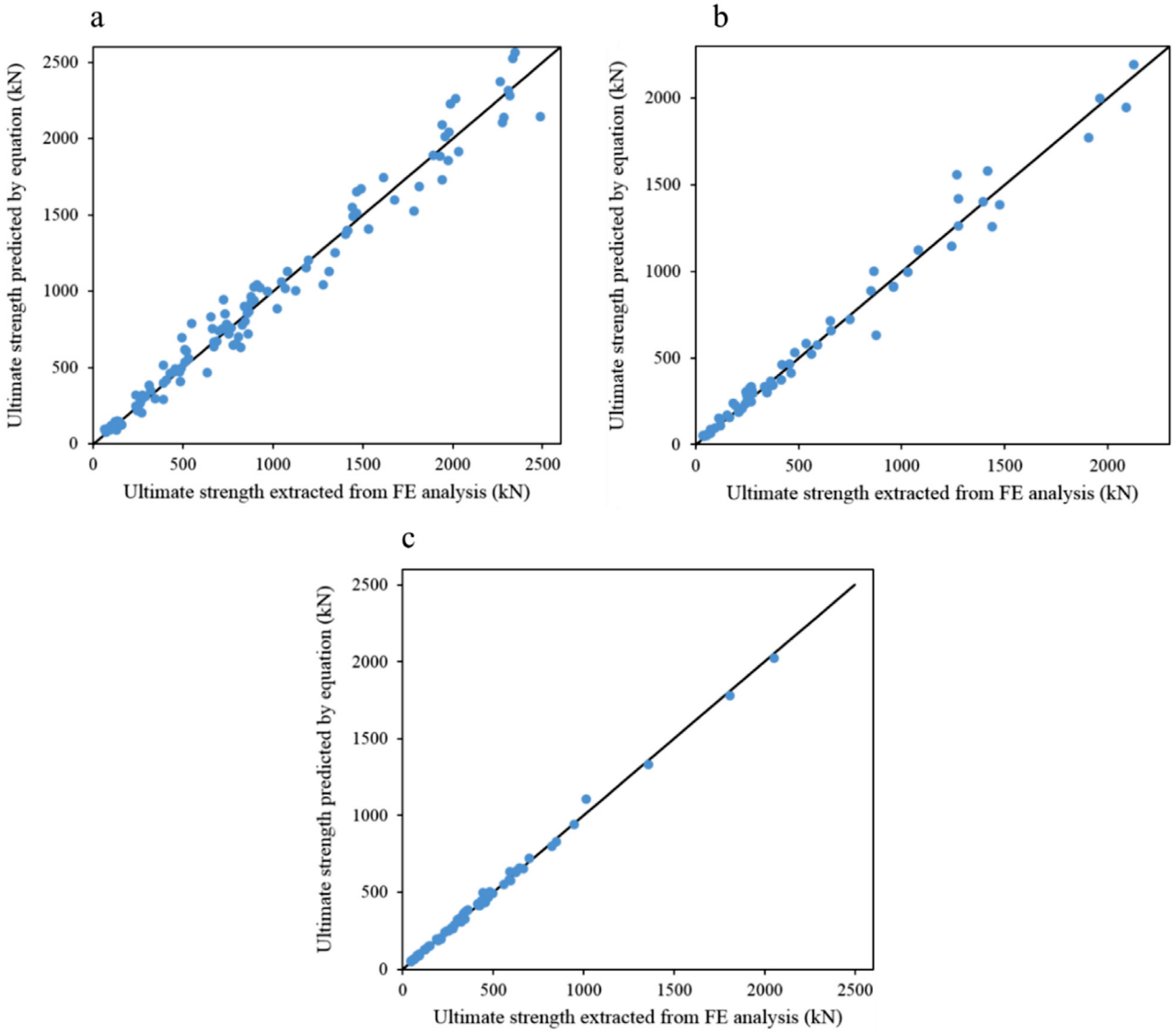

Fig. 27. Comparison of the ultimate strength predicted by the proposed equations with the corresponding training data extracted from FE analyses (the second type of loading): (a) Eq. (7), (b) Eq. (8), and (c) Eq. (9).

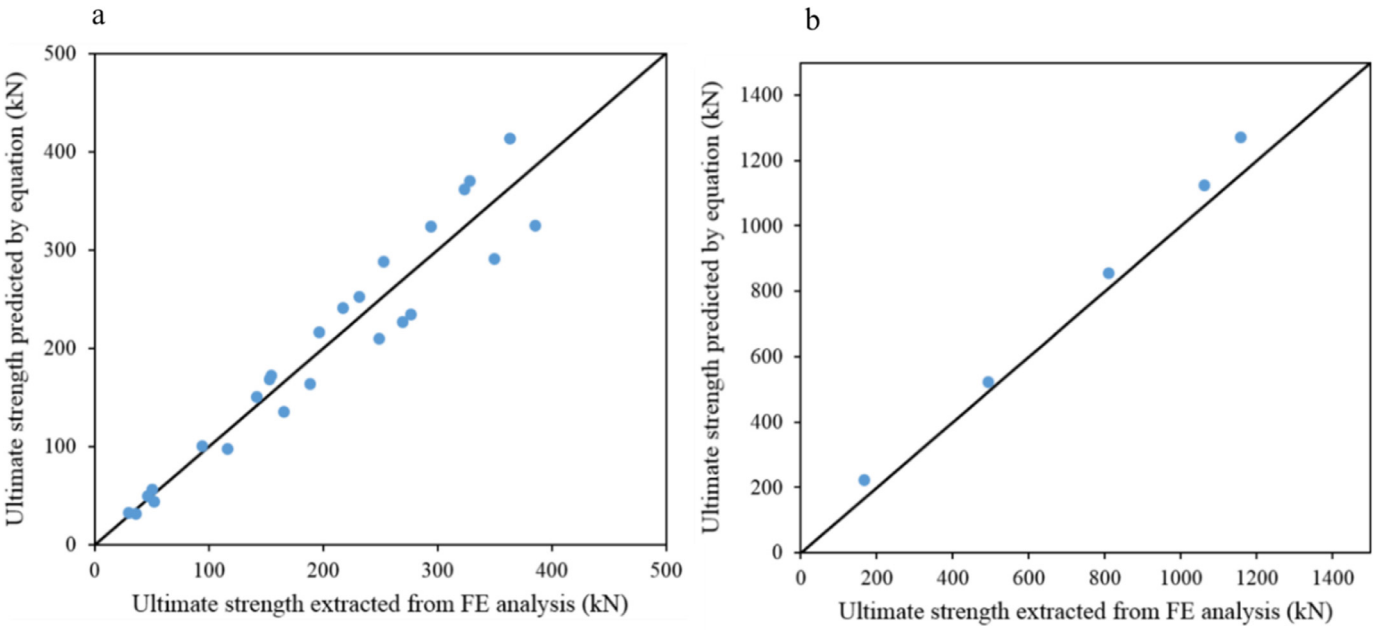

Fig. 28. Comparison of the ultimate strength predicted by the proposed equations with the corresponding test data extracted from FE analyses (the first type of loading): (a) Eq. (4), (b) Eq. (5).

developing the equations, and the remaining data was used for testing the validity of developed equations. After performing a large number of nonlinear analyses by using training dataset, following parametric equations were established for calculating the ultimate strength of two-planar KT-joints at high temperature under two types of loading. For each failure mode, an individual equation was developed. The ultimate strength of the joint is the minimum value between the strength values obtained for different failure modes.

The ultimate strength of two-planar KT-joint under the first type of loading:

(I) Failure mode *A: Chord wall plastification*

$$F_{uA} = 1.604\ Af_y\left(-0.463 + 3.041\ {K_{yT}}^{1.046}\right).\left(1.877 + 1.904\ {K_{ET}}^{-1.065}\right).\left(1.371 + 2.607\ {K_{pT}}^{1.250}\right).\left(1.982 - 1.785\ \beta^{3.240}\right).\left(2.601 - 2.586\ \gamma^{0.001}\right).\left(-2.149 + 2.248\theta^{-0.015}\right).\left(1.714 + 2.297\ \tau^{-1.228}\right) \quad R^2 = 0.963 \tag{4}$$

(II) Failure mode B: Brace local buckling

$$F_{uB} = 1.777\ Af_y\left(3.216 - 0.120\ {K_{yT}}^{4.468}\right).\left(0.366 + 3.587{K_{ET}}^{1.426}\right).\left(2.405 + 2.050\ {K_{pT}}^{-0.127}\right).\left(-2.100 + 2.245\ \beta^{-0.033}\right).\left(2.211 - 2.198\ \gamma^{0.001}\right).\left(2.927 + 1.215\times 10^{-5}\ \theta^{-15.552}\right).\left(2.490 - 1.386\ \tau^{2.941}\right) \quad R^2 = 0.990 \tag{5}$$

$$F_u = \min\{F_{uA}, F_{uB}\} \tag{6}$$

The ultimate strength of two-planar KT-joint under the second type of loading:

(I) Failure mode A: Chord wall plastification

$$F_{uA} = 1.977\ Af_y\left(4.261 + 0.048\ {K_{yT}}^{16.032}\right).\left(1.415 + 4.040{K_{ET}}^{1.552}\right).\left(3.610 - 0.090\ {K_{pT}}^{-1.212}\right).\left(2.682 - 2.540\ \beta^{0.116}\right).\left(2.325 - 2.289\ \gamma^{0.002}\right).\left(-2.870 + 3.026\ \theta^{-0.015}\right).\left(3.424 - 1.964\ \tau^{5.445}\right) \quad R^2 = 0.962 \tag{7}$$

(II) Failure mode B: Brace local buckling

$$F_{uB} = 1.042\ Af_y\left(-0.497 - 0.564\ {K_{yT}}^{0.308}\right).\left(-0.044 + 0.632{K_{ET}}^{0.612}\right).\left(1.173 + 0.905\ {K_{pT}}^{0.254}\right).\left(1.707 + 0.959\ \beta^{-0.456}\right).\left(35.208 - 0.050\ \gamma^{1.558}\right).\left(0.855 - 0.856\ \theta^{-0.0005}\right).\left(0.691 + 1.123\ \tau^{-1.379}\right) \quad R^2 = 0.961 \tag{8}$$

III) Failure mode AB: The combination of wall plastification and brace local buckling

$$F_{uAB} = 1.566\ Af_y\left(3.649 - 0.153\ {K_{yT}}^{-1.551}\right).\left(0.719 + 2.922\ {K_{ET}}^{1.366}\right).\left(0.685 + 3.321\ {K_{pT}}^{0.069}\right).\left(1.195 + 3.710\ \beta^{-0.135}\right).\left(1.741 - 1.705\ \gamma^{0.005}\right).\left(1.948 - 1.937\ \theta^{0.007}\right).\left(1.598 + 2.511\ \tau^{-1.270}\right) \quad R^2 = 0.996 \tag{9}$$

$$F_u = \min\{F_{uA}, F_{uB}, F_{uAB}\} \tag{10}$$

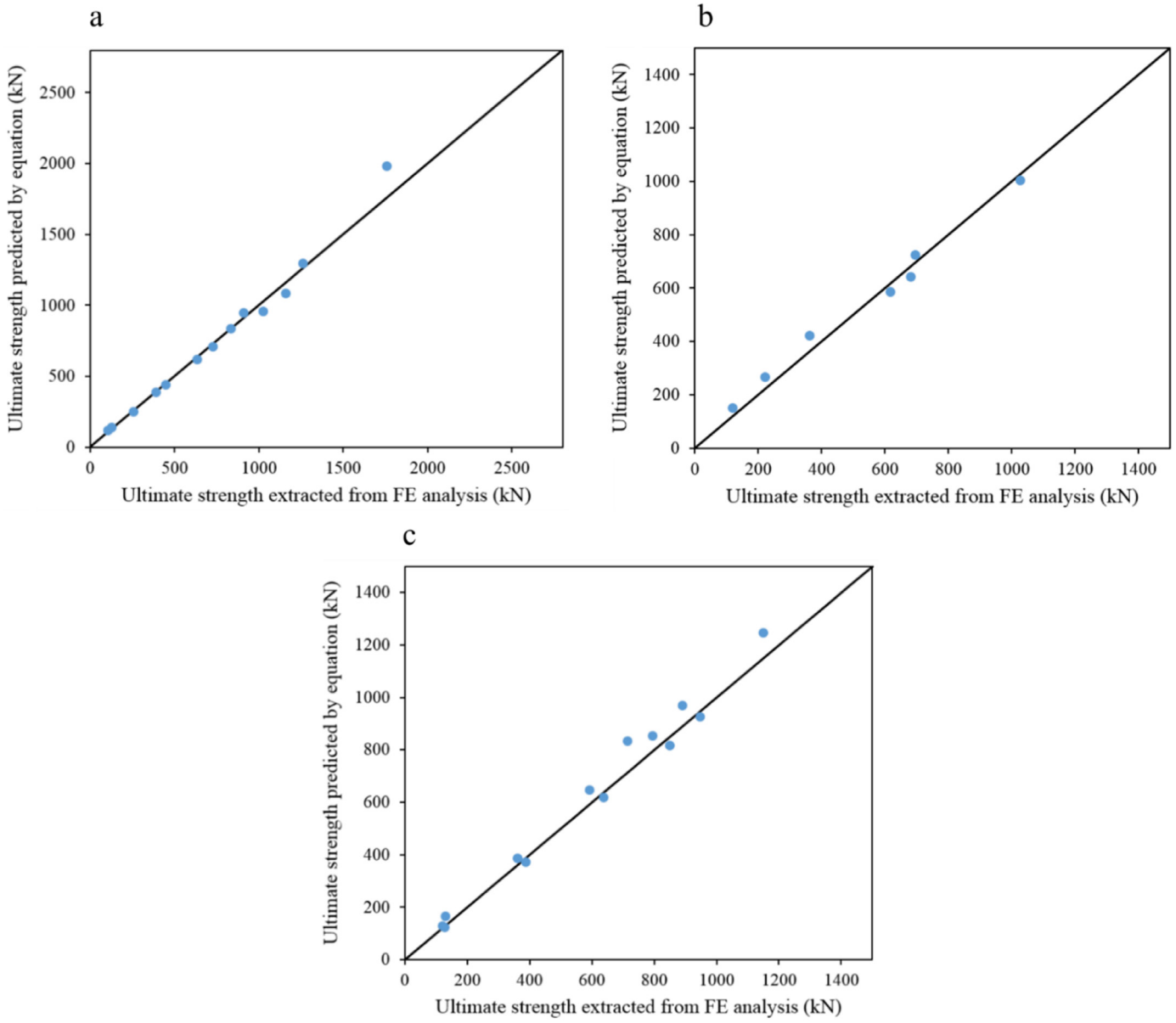

Fig. 29. Comparison of the ultimate strength predicted by the proposed equations with the corresponding test data extracted from FE analyses (the second type of loading): (a) Eq. (7), (b) Eq. (8), and (c) Eq. (9).

In above equations, F_u is the ultimate strength of two-planar KT-joint; A is the cross section area of the brace (i.e. $A = \pi(d^2 - (d-2t)^2)/4$); k_{yT} is the ratio of effective yield stress at elevated temperatures to the yield stress at 20 °C ($k_{yT} = f_{yT}/f_y$); k_{ET} is the ratio of Young's modulus at elevated temperatures to the Young's modulus at 20 °C ($k_{ET} = E_{aT}/E_a$); and k_{PT} is the ratio of the proportional limit at elevated temperatures to the yield stress at 20 °C ($k_{PT} = f_{PT}/f_y$).

The parameter θ should be specified in radians; and R^2 represents the coefficient of determination. The values obtained for R^2 are quite high. The validity ranges of non-dimensional geometrical parameters for the proposed formulas are as follows:

$$\begin{aligned} 30^\circ \le \theta \le 60^\circ \\ 0.3 \le \beta \le 0.6 \\ 10 \le \gamma \le 30 \\ 0.4 \le \tau \le 1.0 \end{aligned} \tag{11}$$

Figs. 26–29 show that there is a good agreement between the results of proposed equations and numerically computed ultimate strength for both training and testing datasets.

The UK Department of Energy [54] proposes a set of assessment criteria concerning the applicability of the parametric formulas. Detailed description of these criteria has been presented and discussed by Azari Dodaran et al. [22,23]. Results of equation assessments based on both training and test-

Table 11
Evaluation of proposed formulas based on the training data set using the UK Department of Energy [50] criteria.

Equation	UK DoE conditions		Decision
	$\%P/R < 0.8$	$\%P/R > 1.5$	
Eq. (4)	4.55% ≤ 5% OK.	0.45% ≤ 50% OK.	Accpet
Eq. (5)	5% ≤ 5% OK.	0% ≤ 50% OK.	Accpet
Eq. (7)	5.13% ≤ 5% OK.	0% ≤ 50% OK.	Accpet
Eq. (8)	1.59% ≤ 5% OK.	0% ≤ 50% OK.	Accpet
Eq. (9)	0% ≤ 5% OK.	0% ≤ 50% OK.	Accpet

Table 12
Evaluation of proposed formulas based on the testing data set using the UK Department of Energy [50] criteria.

Equation	UK DoE conditions		Decision
	$\%P/R < 0.8$	$\%P/R > 1.5$	
Eq. (4)	0% ≤ 5% OK.	0% ≤ 50% OK.	Accpet
Eq. (5)	0% ≤ 5% OK.	0% ≤ 50% OK.	Accpet
Eq. (7)	0% ≤ 5% OK.	0% ≤ 50% OK.	Accpet
Eq. (8)	0% ≤ 5% OK.	0% ≤ 50% OK.	Accpet
Eq. (9)	0% ≤ 5% OK.	0% ≤ 50% OK.	Accpet

ing datasets are presented in Tables 11 and 12. It can be concluded that all of proposed equations satisfy the UK DoE criteria and hence can reliably be used for design purposes.

5. Conclusions

A total of 540 nonlinear FE analyses were performed on 54 models of two-planar CHS KT-joints subjected to two types of axial loading at five different temperatures (20 °C, 200 °C, 400 °C, 550 °C, and 700 °C). The main objective was to study the influence of temperature and dimensionless geometrical parameters (β, γ, θ, and τ) on the ultimate load, failure modes, and initial stiffness of the two-planar KT-joints. A set of design equations was also developed, through nonlinear regression analyses, to calculate the ultimate load of two-planar KT-joints subjected to two types of axial loading at elevated temperatures. Results of the present research can be summarized as follows:

The ultimate load of a two-planar tubular KT-joint under the first type of loading at 200 °C, 400 °C, 550 °C, and 700 °C is, on average, 0.90, 0.70, 0.42, and 0.14 of the joint's ultimate load at ambient temperature, respectively. This means that by increasing the temperature, the reduction of the ultimate strength is 11.11%, 42.86%, 138.10%, and 614.29% at 200 °C, 400 °C, 550 °C, and 700 °C, respectively. The corresponding values for the joints under the second type of loading are 12.36%, 49.25%, 138.19%, and 669.236% at 200 °C, 400 °C, 550 °C, and 700 °C, respectively. These major numbers indicate that the strength reduction in two-planar KT-joints due to the elevated temperatures should not be disregarded especially for the temperatures beyond 400 °C. The reduction of ultimate load of the joints under the first type of loading is smaller than the corresponding values of the joints under the second type of loading.

Considerably high values achieved for the coefficients of determination and the satisfaction of the acceptance criteria recommended by the UK DoE guarantee the accuracy of the proposed equations. Therefore, these formulas can be reliably applied for the design of tubular structures.

Acknowledgments

Useful comments of anonymous reviewers on draft version of this paper are highly appreciated.

References

[1] M. Jin, J. Zhao, M. Liu, J. Chang, J. Constr. Steel Res. 67 (2011) 75–83.
[2] Y.B. Shao, Y. Zheng, H. Zhao, D. Yang, Thin Walled Struct. 98 (2016) 533–546.
[3] E. Ozyurt, Y.C. Wang, Eng. Struct. 88 (2015) 225–240.
[4] K.H. Tan, T.C. Fung, M.P. Nguyen, J. Struct. Eng. 139 (1) (2013) 73–84.
[5] Y. Makino, Y. Kurobane, K. Ochi, in: Proceedings of the Second International Institute of Welding Conference on Welding of Tubular Structures, New York, US, 1984, pp. 451–458.
[6] J.C Paul, Y. Makino, Y. Kurobane. Proceedings of the Second International Offshore and Polar Engineering Conference 1992; 377–383.
[7] M.M.K Lee, S.R. Wilmshurst, J. Constr. Steel Res. 32 (1995) 281–301.
[8] M.M.K Lee, S.R. Wilmshurst, J. Struct. Eng. 122 (8) (1996) 893–904.
[9] N.C.S Forti, J.A.V Requena, T.L.D Fort, J. Constr. Steel Res. 114 (2015) 188–195.
[10] E. Ozyurt, Y.C. Wang, K.H. Tan, Eng. Struct. 59 (2014) 574–586.
[11] J. Wardenier, Y. Kurobane, J.A. Packer, G.J. Van der Vegte, X.L. Zhao, Design Guide for Circular Hollow Section (CHS) Joints Under Predominantly Static Loading, 2nd Edition, CIDECT, Geneva, Switzerland, 2008.
[12] EN 1993-1-8, Eurocode 3: Design of Steel structures, Part 1-8: Design of Joints, British Standards Institute, London, UK, 2005.
[13] M.L. Liu, J.C. Zhao, M. Jin, China Offshore Platform 24 (2009) 17–23 [in Chinese] (Cited by: He SB, Shao YB, Zhang HY, Yang DP, Long, FL. Experimental study on circular hollow section (CHS) tubular K-joints at elevated temperature. Engineering Failure Analysis 2013; 34:204–216).
[14] W. Yu, J. Zhao, H. Luo, J. Shi, D. Zhang, J. Constr. Steel Res. 67 (2011) 1376–1385.
[15] J. Xu, J. Zhao, Z. Song, M. Liu, Saf. Sci. 50 (2012) 1495–1501.
[16] C. Chen, Y.B. Shao, J. Yang, Thin Walled Struct. 92 (2015) 104–114.
[17] F. Gao, X.Q. Guan, H.P. Zhu, X.N. Liu, J. Constr. Steel Res. 115 (2015) 106–120.
[18] T.C. Fung, K.H. Tan, M.P. Nguyen, J. Struct. Eng. (2015) 1–11.
[19] Y.B. Shao, H. Zhao, D. Yang, Adv. Struct. Eng. 20 (5) (2017) 704–721.
[20] Y.B. Shao, S. He, D. Yang, KSCE J. Civ. Eng. 21 (3) (2017) 900–911.
[21] E. Ozyurt, Y.C. Wang, Structures 14 (2018) 15–31.
[22] N. Azari Dodaran, H. Ahmadi, M.A. Lotfollahi-Yaghin, Thin Walled Struct. 130 (C) (2018) 467–486.
[23] N. Azari Dodaran, H. Ahmadi, M.A. Lotfollahi-Yaghin, Mar. Struct. 61 (2018) 282–308.
[24] X. Lan, Y. Huang, T.M. Chan, B. Young, Thin Walled Struct. 122 (2018) 501–509.
[25] S.B. He, Y.B. Shao, H.Y. Zhang, D.P. Yang, F.L. Long, Eng Fail Anal 34 (2013) 204–216.
[26] S. He, Y.B. Shao, H. Zhang, Q. Wang, Fire Saf. 71 (2015) 174–186.
[27] S. He, Y.B. Shao, H. Zhang, J. Constr. Steel Res. 115 (2015) 398–406.
[28] X. Lan, F. Wang, Z. Luo, D. Liu, C. Ning, X. Xu, Adv. Struct. Eng. (2016) 1–11.
[29] X. Lan, Y. Huang, Thin Walled Struct. 108 (2016) 270–279.
[30] Y.B. Shao, Y. Zheng, H. Zhao, D. Yang, Thin Walled Struct. 98 (2016) 533–546.
[31] M. Jin, J. Zhao, J. Chang, M.L. Liu, J. Shanghai Jiaotong Univ. (Chin. Ed.) 16 (1) (2011) 97–104.

[32] M. Jin, J. Zhao, J. Chang, D. Zhang, J. Constr. Steel Res. 70 (2012) 93–100.
[33] C. Chen, Y.B. Shao, J. Yang, J. Constr. Steel Res. 85 (2013) 24–39.
[34] M.L. Liu, J.C. Zhao, M. Jin, J. Constr. Steel Res. 66 (2010) 504–511.
[35] EN 1993-1-2, Eurocode 3: Design of Steel structures, Part 1-2: Structural Fire Design, British Standards Institute, London, UK, 2005.
[36] M. Mirmomeni, A. Heidarpour, X.L. Zhao, C. Hutchinson, J.A. Packer, C. Wu, Int J Impact Eng 76 (2015) 178–188.
[37] F. Azhari, A. Heidarpour, X.L. Zhao, C. Hutchinson, Thin Walled Struct. 119 (2017) 114–125.
[38] F. Azhari, A.A. Hossain Apon, A. Heidarpour, X.L. Zhao, C. Hutchinson, Constr. Build. Mater. 175 (2018) 790–803.
[39] M.M.K. Lee, J. Constr. Steel Res. 51 (1999) 265–286.
[40] T.C. Fung, C.K. Soh, W.M. Gho, F. Qin, J. Constr. Steel Res. 57 (2001) 855–880.
[41] F. Javidan, A. Heidarpour, X.L. Zhao, J. Minkkinen, Eng. Struct. 118 (2016) 16–27.
[42] M. Efthymiou, PKER Report (1985) 185–199.
[43] P. Smedley, P. Fisher, in: Proceedings of the International Offshore and Polar Engineering Conference, Edinburg, UK, 1991.
[44] M.R. Morgan, M.M.K. Lee, J. Constr. Steel Res. 45 (1) (1998) 67–97.
[45] Y.S. Choo, X.D. Qian, J. Wardenier, J. Constr. Steel Res. 62 (2006) 316–328.
[46] ANSYS Inc, ANSYS Ver. 17 Documentation: Elements Reference, Canonsburg, Pennsylvania, US, 2016.
[47] W.F. Cofer, K.M. Will, Eng. Comput. 9 (1992) 345–358.
[48] E. Dexter, M. Lee, J. Struct. Eng. 125 (2) (1999) 194–201.
[49] X.D. Qian, Y.S. Choo, J.Y. Liew, J. Wardenier, J. Struct. Eng. 131 (2005) 768–780.
[50] X. Ma, W. Wang, Y. Chen, X. Qian, J. Constr. Steel Res. 114 (2015) 217–236.
[51] B. Gu, X. Qian, A. Ahmed, Front. Struct. Civ. Eng. 10 (3) (2016) 345–362.
[52] P. Kohnke, Theory Reference For the Mechanical APDL and Mechanical Applications, ANSYS Inc., Release 12 2009.
[53] L.H. Lu, G.D. De Winkel, Y. Yu, J. Wardenier, in: The 6th International Symposium on Tubular Structures, Melbourne, Australia, 1994.
[54] UK Department of Energy (DoE), Background Notes to the Fatigue Guidance of Offshore Tubular Joints, London, UK, 1983.